JOURNAL OF COMPUTATIONAL PHYSICS 117, 332–349 (1995)

Particle Method for Turbulent Flows: Integration of Stochastic Model Equations

S. B. POPE

Sibley School of Mechanical and Aerospace Engineering, Cornell University, Ithaca, New York 14853

Received February 18, 1992

A numerical method is developed to integrate the stochastic differential equations that arise in a particle method for modelling turbulent flows. These equations present several challenges, the foremost being the presence of multiple time scales, the smallest of which can be significantly less than an acceptable time-step size, Δt. The essence of the approach adopted is to transform and decompose the equations so that the stochastic components (which contain the small time scales) appear as strictly linear stochastic differential equations. Analytic solutions to these equations (with frozen coefficients) are then exploited to produce a stable and accurate scheme. When the method is used to advance the properties of N particles, the resulting numerical error can be decomposed into three contributions: statistical error, bias, and time-stepping error. Comprehensive tests to study these errors are reported for two test cases. A novel variance-reduction technique is described that significantly reduces the statistical error, which scales as $N^{-1/2}$. In general, the bias is smaller, and scales as N^{-1} (in accord with a simple analysis). The time-stepping error is less than 1% for a non-dimensional time step of $\frac{1}{32}$—which may be several times larger than the smallest time scale. Over the range of time-step size investigated, the dominant time-stepping error varies as $\Delta t^{3/2}$. The method has the requisite stability, accuracy, and efficiency for incorporation in multi-dimensional particle methods.

1. INTRODUCTION

There is continuing progress in the development and application of turbulence models to calculate the properties of turbulent flows of engineering significance [1, 2]. Flows of different complexity require turbulence models providing different levels of description of the turbulent phenomena. Most industrial and commercial turbulent-flow codes are based on (at most) a two-equation turbulence model, such as $k - \varepsilon$ [3, 4]. Several different and significant shortcomings of two-equation models have been known for over a decade [5], thus motivating the development of models that provide a fuller description of the turbulence. For chemically inert flows, Reynolds-stress (or second-moment) closures (e.g., [6]) can provide significant improvements. For reactive flows (especially combustion) pdf methods [7–11] have the overwhelming advantage of representing reaction exactly—without modeling assumptions. Even for inert flows, pdf methods have several advantages, such as treating convective transport exactly and representing the distribution of turbulent scales [12, 13, 11].

Moment closures (i.e., $k - \varepsilon$ or Reynolds-stress) result in a set of about 10 partial differential equations, which are solved numerically by finite-volume methods. While these models have been used for 20 years, there has continually been concern about the level of numerical error in the computed solutions (e.g., [14]). Over the years, improved numerical methods have been developed (e.g., [15, 16]), and faster computers have allowed finer grids to be used. While it is probable that accurate numerical solutions can now be obtained (at least in two dimensions), there is regrettably little or no incontrovertible evidence to support this opinion.

Compared to moment-closure model equations, the modelled, pdf equations have a completely different structure, and different numerical solution techniques are employed. Specifically, Monte Carlo methods are used in which the pdf is represented by an ensemble of particles. In the first method developed [17] the particles are located at grid nodes in physical space, whereas in a later method [8] (now preferred) the particles are continuously distributed. In application to simple flows, the convergence and accuracy of these methods have been demonstrated [17–19]. The methods have also been applied to several, complex 2D and 3D flows (e.g., [20–25]).

These numerical solutions of the modelled pdf equations have demonstrated the favorable attributes of pdf methods for turbulent flows (both with and without reaction), and they have proved the feasibility of applying the method to complex 2D and 3D flows. At the same time they have also revealed the need, benefit, and possibility of a more accurate and efficient numerical method. This paper reports the first step in the development of such an improved particle method.

The numerical method developed here is for the modelled equation for the joint pdf of velocity and turbulence frequency [12, 13, 11]. This single equation provides a complete model: that is, apart from fluid properties and initial and boundary conditions, no additional inputs are required. This is in contrast to pdf methods based on the joint pdf of compositions (or of velocity and compositions) which require additional turbulence-model equations. Consequently, for the velocity-frequency joint

0021-9991/95 $6.00

pdf equation considered here, a self-contained particle method can be developed, rather than the hybrid particle/finite-difference methods necessitated by incomplete pdf models.

A particle method for multi-dimensional non-reactive flows requires three basic ingredients: an integration scheme to advance the particle properties in time; a method of representing mean fields (e.g., the mean velocity fields), and of estimating them from the particle properties; and an algorithm to determine the mean pressure field and to enforce the mean continuity equation. For flows with complex reactions (e.g., combustion) a fourth required ingredient is an efficient means of incorporating the effects of reaction on the particle compositions. The contribution of the present work is to provide the first ingredient. That is, we develop and demonstrate here an accurate numerical method for the time-integration of the stochastic differential equations for the particle velocity and frequency. This aspect of the overall problem is isolated by restricting attention to inert statistically homogeneous turbulence. Nevertheless, the method is developed with the extension to the general case in mind.

The accurate numerical integration of stochastic differential equations (sde's) is much more difficult than the corresponding task for ordinary differential equations (ode's); and a specialized literature on the topic has emerged (see, e.g., [26–30]). The standard problem generally considered is of the form: given coefficients $a(x, t)$ and $b(x, t)$, an initial condition $X(0) = x_0$, and a stopping time $T > 0$, integrate the stochastic differential equation,

$$dX(t) = a(X(t), t)\,dt + b(X(t), t)\,dW(t), \tag{1}$$

to obtain $X(T)$. Here $W(t)$ is a Wiener process.

The problem encountered here, however, is somewhat different. Some of the ingredients are contained in the following model problem: given coefficients (different from those above) $a(x, y)$ and $b(x, y)$, a function $Y(x)$, an initial condition $X(0) = x_0$, and a stopping time $T > 0$, integrate the stochastic differential equation

$$dX(t) = a(X(t), \langle Y(X(t))\rangle)\,dt + b(X(t), \langle Y(X(t))\rangle)\,dW(t), \tag{2}$$

to obtain $X(T)$. The essential difference between (1) and (2) is that in (2) the coefficients depend on the mean of a function of the process, i.e., $\langle Y(X(t))\rangle$.

Instead of standard techniques applied to (1), here, by exploiting the particular structure of the sde's we use a different approach, namely, to transform and decompose the equations so that (on each time step) the stochastic components can be advanced by an approximate *analytic* solution. This leads to a two-stage predictor–corrector scheme that is both accurate and robust (i.e., stable for very large time steps). In addition, novel variance-reduction techniques are described that reduce the statistical error involved in estimating means (e.g., $\langle Y(X(t))\rangle$) from a finite ensemble of samples.

The stochastic turbulence-model equations are presented in the next section, and then an overview of the particle method is provided in Section 3. In the following two sections the time-integration schemes are presented for the frequency and for the velocity equations. Two test cases are considered: sheared Gaussian turbulence (for which there is an analytic solution) and a more severe test with bimodal initial conditions. Results for these cases (reported in Section 6) clearly demonstrate the stability, convergence, accuracy, and efficiency of the method. The paper closes with discussion and conclusions.

2. STOCHASTIC MODEL EQUATIONS

Before presenting the model equations, the class of flows considered is defined and the notation is introduced.

We consider constant-density, homogeneous turbulence. At position $\mathbf{x}$ and time t the fluid velocity $\mathbf{U}(\mathbf{x}, t)$—which is a random variable—can be decomposed into its mean (or mathematical expectation) $\langle \mathbf{U}(\mathbf{x}, t)\rangle$ and fluctuation $\mathbf{u}(\mathbf{x}, t)$:

$$\mathbf{U}(\mathbf{x}, t) = \langle \mathbf{U}(\mathbf{x}, t)\rangle + \mathbf{u}(\mathbf{x}, t). \tag{3}$$

Without loss of generality (for homogeneous turbulence) we take $\langle \mathbf{U}\rangle$ to be zero at the origin ($\langle \mathbf{U}(0, t)\rangle = 0$). Then, since a necessary condition for homogeneity is the linearity of $\langle \mathbf{U}\rangle$ in $\mathbf{x}$, the mean velocity field is fully described by the velocity-gradient tensor

$$\Gamma_{ij}(t) = \frac{\partial}{\partial x_j}\langle U_i(\mathbf{x}, t)\rangle. \tag{4}$$

In view of homogeneity, the Reynolds stresses $\langle u_i u_j\rangle$ and the turbulent kinetic energy ($k \equiv \frac{1}{2}\langle u_i u_i\rangle$) depend on t only.

With ν being the kinematic viscosity, the pseudo-dissipation is defined by

$$\varepsilon(\mathbf{x}, t) = \nu \frac{\partial u_i}{\partial x_j}\frac{\partial u_i}{\partial x_j}, \tag{5}$$

and then the turbulence relaxation rate or *frequency* is defined by

$$\omega(\mathbf{x}, t) = \varepsilon(\mathbf{x}, t)/k(t). \tag{6}$$

It may be noted that $\omega(\mathbf{x}, t)$ is non-negative.

In the model considered [12, 13], the fundamental representation of the turbulence is the (one-point, one-time, Eulerian) joint pdf of the fluctuating velocity ($\mathbf{u}$) and frequency (ω), which is denoted by $f(\mathbf{v}, \theta; t)$. Here $\mathbf{v} = \{v_1, v_2, v_3\}$ and θ are sample-space variables corresponding to $\mathbf{u}$ and ω. Thus $f(\mathbf{v}, \theta; t)$ is the probability density of the compound event $\{\mathbf{u}(\mathbf{x}, t) = \mathbf{v}, \omega(\mathbf{x}, t) = \theta\}$.

Moments, and other means, can be obtained by integrating the joint pdf. For example,

$$\int_S f(\mathbf{v}, \theta; t)\mathbf{v}\, d\mathbf{v}\, d\theta = \langle \mathbf{u}(\mathbf{x}, t)\rangle = 0, \tag{7}$$

$$\int_S f(\mathbf{v}, \theta; t)\theta\, d\mathbf{v}\, d\theta = \langle \omega(t)\rangle, \tag{8}$$

and

$$\int_S f(\mathbf{v}, \theta; t)v_i v_j\, d\mathbf{v}\, d\theta = \langle u_i u_j\rangle, \tag{9}$$

where $\int_S(\quad)\, d\mathbf{v}\, d\theta = \int_0^\infty \int_{-\infty}^\infty \int_{-\infty}^\infty \int_{-\infty}^\infty (\quad)\, dv_1\, dv_2\, dv_3\, d\theta$ denotes integration over the whole sample space. It is also convenient to define *frequency-weighted* means, which are indicated by a tilde; for example,

$$\tilde{u}_i \equiv \langle u_i\omega\rangle/\langle\omega\rangle \tag{10}$$

and

$$\tilde{k} \equiv \tfrac{1}{2}\langle u_i u_i \omega\rangle/\langle\omega\rangle. \tag{11}$$

A Lagrangian approach is taken both in the modelling and in the numerical method. With $\mathbf{x}^+(t)$ being the position of a fluid particle at time t, other fluid-particle properties are defined by, for example,

$$\mathbf{u}^+(t) \equiv \mathbf{u}(\mathbf{x}^+(t), t) \tag{12}$$

and

$$\omega^+(t) \equiv \omega(\mathbf{x}^+(t), t). \tag{13}$$

For constant-density homogeneous turbulence, one-point one-time Eulerian and Lagrangian statistics are identical [8]. Consequently $f(\mathbf{v}, \theta; t)$ is also the joint pdf of $\mathbf{u}^+(t)$ and $\omega^+(t)$; and in particular we have $\langle\omega^+(t)\rangle = \langle\omega(\mathbf{x}, t)\rangle$ and $\langle u_i^+(t)u_j^+(t)\rangle = \langle u_i u_j\rangle$.

The idea of the stochastic Lagrangian modelling approach is to construct stochastic processes $\mathbf{u}^*(t)$ and $\omega^*(t)$ that model the corresponding fluid-particle properties, $\mathbf{u}^+(t)$ and $\omega^+(t)$. In the model of Pope and Chen [12, 13], $\omega^*(t)$ evolves according to the Ito stochastic differential equation [31]

$$\begin{aligned} d\omega^* = &-\omega^*\langle\omega\rangle\, dt\left\{S_\omega + C_\chi\left[\ln\left(\frac{\omega^*}{\langle\omega\rangle}\right) - \mathscr{L}\right]\right\} \\ &+ \langle\omega\rangle^2 h\, dt + \omega^*(2C_\chi\langle\omega\rangle\sigma^2)^{1/2}\, dW. \end{aligned} \tag{14}$$

In this equation, $d\omega^*(t) = \omega^*(t + dt) - \omega^*(t)$ is the infinitesimal increment in ω^*; $dW(t)$ is the increment of a Wiener process $W(t)$ which has the properties

$$\langle dW\rangle = 0, \quad \langle (dW)^2\rangle = dt; \tag{15}$$

and the coefficients are defined by

$$S_\omega = -\tfrac{1}{4}C_{\omega 1}(\Gamma_{ij} + \Gamma_{ji})(\Gamma_{ij} + \Gamma_{ji})/\langle\omega\rangle^2 + C_{\omega 2}, \tag{16}$$

$$\mathscr{L} = \left\langle \frac{\omega}{\langle\omega\rangle}\ln\left(\frac{\omega}{\langle\omega\rangle}\right)\right\rangle, \tag{17}$$

$$\begin{aligned} h &= C_{\omega 3}(1 - \mu_{1/2}/\mu_{1/2G})^2, \quad && \mu_{1/2} \leqq \mu_{1/2G}, \\ &= 0, && \mu_{1/2} > u_{1/2G}, \end{aligned} \tag{18}$$

where

$$\mu_{1/2} = \left\langle \left(\frac{\omega}{\langle\omega\rangle}\right)^{1/2}\right\rangle \tag{19}$$

and

$$\mu_{1/2G} = e^{-\sigma^2/8}. \tag{20}$$

The model constants are ascribed the values $\sigma^2 = 1.0$, $C_\chi = 1.6$, $C_{\omega 1} = 0.04$, $C_{\omega 2} = 0.9$, and $C_{\omega 3} = 1.0$. (Here and below, the notation has been simplified by omitting asterisks within means. That is, $\langle\omega\rangle$ is written for $\langle\omega^*\rangle$ etc.)

The velocity model is the stochastic differential equation

$$du_i^* = -\Gamma_{ij}u_j^*\, dt + D_i(\mathbf{u}^*, \omega^*, t)\, dt + (C_0\tilde{k}\omega^*)^{1/2}\, dW_i, \tag{21}$$

where $\mathbf{W}(t)$ is an isotropic vector-valued Wiener process (independent of that in the ω^* equation), the increments of which satisfy

$$\langle d\mathbf{W}\rangle = 0, \quad \langle dW_i\, dW_j\rangle = dt\, \delta_{ij}. \tag{22}$$

The drift term $\mathbf{D}$ is given by

$$\begin{aligned} D_i(\mathbf{u}^*, \omega^*, t) = &-\left(\frac{1}{2} + \frac{3}{4}C_0\right)\langle\omega\rangle\frac{\tilde{k}}{k}u_i^* + G_{ij}^a u_j^* \\ &- \frac{3}{4}C_0\tilde{A}_{ij}^{-1}(\omega^* u_j^* - \langle\omega u_j\rangle) \\ &+ \frac{3}{4}C_0\frac{\tilde{k}}{k}A_{ij}^{-1}\langle\omega\rangle u_j^*. \end{aligned} \tag{23}$$

Here $\mathbf{A}$ is the normalized Reynolds-stress tensor

$$A_{ij} = 3\langle u_i u_j\rangle/\langle u_m u_m\rangle, \tag{24}$$

and $\tilde{\mathbf{A}}$ is its ω-weighted counterpart

$$\tilde{A}_{ij} = 3\langle\omega u_i u_j\rangle/\langle\omega u_m u_m\rangle. \tag{25}$$

Then A_{ij}^{-1} denotes the $i - j$ component of the inverse $\mathbf{A}^{-1}$. (A

detail—inconsequential here—is that $\mathbf{A}^{-1}$ is the "modified determinant" inverse (see [12]) which is finite even for singular $\mathbf{A}$.) Finally, G^a_{ij}—here taken to be zero—is a modelled tensor function of $\mathbf{A}_{ij}$ and $\mathbf{\Gamma}_{ij}$; a specific form is given by Haworth and Pope [32, 33] and other specifications are comprehensively discussed by Pope [34]. The single model constant appearing in the equation is $C_0 = 3.5$.

The physics embodied in these model equations is described in the original works [12, 13] and reviewed in [11] and is not discussed further here.

The joint pdf of $\mathbf{u}^*(t)$ and $\omega^*(t)$, denoted by $f^*(\mathbf{v}, \theta; t)$, is a model for the pdf of the fluid properties $f(\mathbf{v}, \theta; t)$. By standard techniques [31, 8] from Eqs. (12) and (19), the evolution equation for f^* is deduced to be

$$\frac{\partial f^*}{\partial t} = \frac{\partial}{\partial v_i}\{f^*\Gamma_{ij}v_j - f^*D_i(\mathbf{v}, \theta, t)\} + \frac{1}{2}C_0\tilde{k}\theta\frac{\partial^2 f^*}{\partial v_i\,\partial v_i} + \langle\omega\rangle\frac{\partial}{\partial\theta}\left\{f^*\theta\left[S_\omega + C_\chi\left(\ln\left(\frac{\theta}{\langle\omega\rangle}\right) - \mathcal{L}\right)\right]\right\} - \langle\omega\rangle^2 h\frac{\partial f^*}{\partial\theta} + C_\chi\langle\omega\rangle\sigma^2\frac{\partial^2}{\partial\theta^2}(f^*\theta). \tag{26}$$

From a given initial condition $f^*(\mathbf{v}, \theta; 0)$, and for a specified imposed mean velocity gradient $\Gamma_{ij}(t)$, this single equation determines the joint pdf $f^*(\mathbf{v}, \theta; t)$ at future times. The remaining coefficients in the equation (i.e., D_i, k, ω, S_w, $\mathcal{L}$ and h) can be expressed in terms of integrals of f^*, for example,

$$\mathcal{L}(t) = \int_S f^*(\mathbf{v}, \theta; t)\frac{\theta}{\langle\omega\rangle}\ln\left(\frac{\theta}{\langle\omega\rangle}\right)d\mathbf{v}\,d\theta \tag{27}$$

(with $\langle\omega\rangle$ being obtained as the integral of θ).

For the stochastic processes $\mathbf{u}^*(t)$ and $\omega^*(t)$, the boundary values ($u_i^* = \pm\infty$, $\omega^* = 0$, and $\omega^* = \infty$) are unattainable. Consequently, Eq. (26) does not require boundary conditions (see Karlin and Taylor [35]).

3. PARTICLE METHOD

The numerical method developed here is a particle method that provides an approximate numerical solution to the modelled joint pdf evolution equation, Eq. (26). The pdf $f^*(\mathbf{v}, \theta; t)$ is represented by an ensemble of N stochastic particles (typically $N = 100$–$10{,}000$) which model fluid particles. At time t the nth stochastic particle has velocity $\mathbf{u}^{(n)}(t)$ and frequency $\omega^{(n)}(t)$. The initial particle properties $(\mathbf{u}^{(n)}(0), \omega^{(n)}(0); n = 1, 2, \ldots, N)$ are independent random samples from the specified initial joint pdf $f^*(\mathbf{v}, \theta; 0)$. Subsequently each particle evolves according to the stochastic model equations—$\mathbf{u}^{(n)}(t)$ according to Eq. (21) and $\omega^{(n)}(t)$ according to Eq. (14). These stochastic differential equations are integrated in time numerically in uniform time steps Δt. (It is convenient to define particle properties in continuous time by linear interpolation between the discrete time levels $j\Delta t$, integer $j \geq 0$. The restriction to uniform time steps is readily removed.)

A basic requirement of the numerical method—*convergence*—is that it converges to the true solution as $N \to \infty$ and $\Delta t \to 0$. From the particle properties we define the discrete pdf by

$$f_N(\mathbf{v}, \theta; t) \equiv \frac{1}{N}\sum_{n=1}^{N}\delta(\mathbf{u}^{(n)}(t) - \mathbf{v})\,\delta(\omega^{(n)}(t) - \theta), \tag{28}$$

where $\delta(\mathbf{v})$ is written for the Dirac delta-function product $\delta(v_1)\,\delta(v_2)\,\delta(v_3)$. It is reasonable to require that f_N converge in distribution to f^*. But since such convergence is extremely difficult to test numerically, we require instead convergence (in mean square) of expectations. Consequently, for all test functions $Q(\mathbf{v}, \theta)$ for which the mean

$$\langle Q(\mathbf{u}(t), \omega(t))\rangle = \int_S Q(\mathbf{v}, \theta)f(\mathbf{v}, \theta; t)\,d\mathbf{v}\,d\theta \tag{29}$$

exists, we define the ensemble mean by

$$\langle Q(\mathbf{u}(t), \omega(t))\rangle_N = \int_S Q(\mathbf{v}, \theta)f_N(\mathbf{v}, \theta; t)\,d\mathbf{v}\,d\theta = \frac{1}{N}\sum_{n=1}^{N}Q(\mathbf{u}^{(n)}(t), \omega^{(n)}(t)). \tag{30}$$

Then we require $\langle Q\rangle_N$—which is a random variable—to converge to $\langle Q\rangle$ in mean square, i.e.,

$$\lim_{\Delta t\to 0}\lim_{N\to\infty}\langle(\langle Q\rangle_N - \langle Q\rangle)^2\rangle = 0. \tag{31}$$

If a convergent numerical method (with given N and Δt) is used to obtain $\langle Q\rangle_N$ at a fixed time t, the resulting numerical error can be decomposed into three contributions:

$$\langle Q\rangle_N - \langle Q\rangle = T_Q(t, \Delta t) + B_Q(t, N, \Delta t) + N^{-1/2}\xi S_Q(t, N, \Delta t). \tag{32}$$

The first contribution is the time-stepping error defined as

$$T_Q(t, \Delta t) = \langle Q\rangle_\infty - \langle Q\rangle, \tag{33}$$

where $\langle Q\rangle_\infty$ is written for $\lim_{N\to\infty}\langle Q\rangle_N$.

The bias B_Q is the deterministic error caused by N being finite:

$$B_Q(t, N, \Delta t) = \langle\langle Q\rangle_N\rangle - \langle Q\rangle_\infty. \tag{34}$$

A necessary condition for convergence is that B_Q tends to zero as N tends to infinity. (In practice, $\langle\langle Q\rangle_N\rangle$ is determined (to a specified confidence) by averaging over independent trials.)

The final contribution is the random—or statistical—error $N^{-1/2}\xi S_Q$. Here ξ is a standardized random variable (i.e., $\langle\xi\rangle = 0$, $\langle\xi^2\rangle = 1$), and the standard error S_Q is defined in terms of the variance of $\langle Q\rangle_N$:

$$S_Q(t, N, \Delta t)^2 = N \operatorname{var}(\langle Q\rangle_N). \tag{35}$$

Asymptotically, as N tends to infinity, S_Q becomes independent of N.

There are two primary considerations in the construction of the numerical method. The first is the time stepping strategy; that is, the method used to integrate the stochastic differential equations for each time step. The second is the use of *variance reduction* techniques [36, 37] to reduce S_Q and, hence, the number of particles required for a given accuracy.

Means, such as $\langle u_i u_j\rangle$ and $\langle\omega\rangle$, change on time scales proportional to $\langle\omega\rangle^{-1}$. It is found, as expected, that accurate solutions are obtained only if the time step is chosen so that $\langle\omega\rangle\,\Delta t$ is small compared to unity. But it is important to recognize that the stochastic differential equations contain a second time scale, proportional to $1/\omega^{(n)}$ (for the nth particle). For Gaussian homogeneous turbulence (see [13]) $\omega^{(n)}$ is log-normally distributed with $\ln\omega^{(n)}$ having variance $\sigma^2 = 1$. Hence, out of an ensemble of 10^5 particles, say, it can be estimated that the maximum value of $\omega^{(n)}$ is likely to be about $40\langle\omega\rangle$—but there is no absolute upper bound. It is highly desirable—and we find it possible—to develop a scheme that for accuracy and stability does not require $\omega^{(n)}\,\Delta t < 1$ for all n.

A predictor–corrector method is used, which, in advancing from time level j ($t_j = j\,\Delta t$) to level $j + 1$ involves the following steps:.

1. The coefficients in the stochastic differential equations are evaluated from ensemble means, based on the particle properties at t_j.

2. The stochastic differential equations are integrated to yield the predictor values at t_{j+1}, denoted by $\hat{\mathbf{u}}^{(n)}(t_{j+1})$ and $\hat{\omega}^{(n)}(t_{j+1})$.

3. The coefficients are evaluated based on $\hat{\mathbf{u}}^{(n)}(t_{j+1})$ and $\hat{\omega}^{(n)}(t_{j+1})$ and averaged with those computed in step 1 to yield second-order accurate approximations to the coefficients at $t_{1/2} = \frac{1}{2}(t_j + t_{j+1})$.

4. Using the predictor particle properties and the coefficients at $t_{1/2}$, the sde's are integrated from t_j to t_{j+1} to yield the new particle properties, $\mathbf{u}^{(n)}(t_{j+1})$ and $\omega^{(n)}(t_{t+1})$.

For ordinary differential equations, this predictor–corrector scheme is second-order accurate; that is, for fixed t, the time-stepping error T_Q varies asymptotically at Δt^2. For the sde's considered here it is found that the dominant time-stepping error varies as $\Delta t^{3/2}$.

It is important to observe that the sde's integrated are not precisely those stated in the previous section for the coefficients are based on ensemble means rather than on expectations. Thus the coefficients have random fluctuations (of order $N^{-1/2}$), which (among other effects) are responsible for the bias. For large N it is found that the bias varies as N^{-1} and, hence, is negligible compared to the random error.

Variance reduction techniques are used to reduce the random error, which arises from three sources: from the initial conditions, from the Wiener processes, and from fluctuations in the coefficients. (While the fluctuations in the coefficients ultimately stem from the other two sources, it is nevertheless useful to consider it as a separate source.) The technique used is to *eliminate* the first two sources of statistical error in certain *controlled moments*, namely $\langle\mathbf{u}\rangle$, $\langle\omega\rangle$, and $\langle u_i u_j\rangle$. The simple way in which this is achieved for the initial conditions is now described.

Let $\hat{\mathbf{u}}^{(n)}(0)$ and $\hat{\omega}^{(n)}(0)$ ($n = 1, 2, ..., N$) be independent samples from the specified initial distribution $f^*(\mathbf{v}, \theta; 0)$. An additive correction to the velocities,

$$\hat{\mathbf{u}}^{(n)}(0) = \hat{\mathbf{u}}^{(n)}(0) + \mathbf{u}^0, \tag{36}$$

and a multiplicative correction to the frequency,

$$\omega^{(n)}(0) = e^c\hat{\omega}^{(n)}(0), \tag{37}$$

is then performed to yield $\langle\omega\rangle_N = \langle\omega\rangle$ and $\langle\hat{\mathbf{u}}\rangle = \langle\mathbf{u}\rangle = 0$. (This uniquely defines the constants $\mathbf{u}^0$ and c, which are of order $N^{-1/2}$.) The velocities are then further corrected to

$$u_i^{(n)}(0) = (\delta_{ij} + L_{ij})\hat{u}_j^{(n)}(0), \tag{38}$$

where L_{ij} is a lower triangular matrix (whose elements are of order $N^{-1/2}$) uniquely determined by the requirement $\langle u_i u_j\rangle_N = \langle u_i u_j\rangle$. Thus by these simple (order $N^{-1/2}$) adjustments the statistical error in the controlled moments is eliminated from the initial conditions.

4. NUMERICAL INTEGRATION OF FREQUENCY

The fundamental idea behind the numerical integration schemes developed for $\omega^*(t)$ here, and for $\mathbf{u}^*(t)$ in the next section, is to transform and decompose the equations so that the stochastic component corresponds to an Ornstein–Uhlenbeck (OU) process [35, 38, 31]. Since an OU process can be described analytically, the numerical integration of the stochastic component is completely avoided and, since the OU process is stationary, the solution is stable for arbitrarily large time steps.

Starting at the general time level $t_j = j\,\Delta t$, the known frequency of the general particle is $\omega^*(t_j)$ and the task is to integrate Eq. (14) to determine $\omega^*(t_{j+1})$ (or $\hat{\omega}(t_{j+1})$ on the predictor step).

The first transformation involves the normalized time τ,

$$\tau(t) \equiv \int_{t_j}^{t} \langle\omega(t')\rangle\, dt'. \tag{39}$$

The start of the time step is $\tau(t_j) = 0$, the end is denoted by $\bar{\tau} = \tau(t_{j+1})$, and the mid-time is $\tau_{1/2} \equiv \frac{1}{2}\bar{\tau}$.

An infinitesimal increment in τ is, for example, $d\omega(\tau) = \omega(\tau + d\tau) - \omega(\tau)$, and W_τ denotes a Wiener process in τ, which has the infinitesimal variance

$$\langle dW_\tau(\tau)^2 \rangle = d\tau = \langle \omega \rangle \, dt. \tag{40}$$

With these definitions Eq. (14) becomes

$$\begin{aligned} d\omega^*(\tau) = &-\omega^* \, d\tau \left\{ S_\omega + C_\chi \left[\ln\left(\frac{\omega^*}{\langle\omega\rangle}\right) - \mathcal{L} \right] \right\} \\ &+ \langle\omega\rangle h \, d\tau + \omega^* (2C_\chi \sigma^2)^{1/2} \, dW_\tau(\tau). \end{aligned} \tag{41}$$

Next, $\omega^*(\tau)$ is decomposed as

$$\omega^*(\tau) \equiv \Omega(\tau) z(\tau) + g(\tau), \tag{42}$$

where

$$g(\tau) \equiv \int_{\tau_{1/2}}^{\tau} \langle \omega(\tau') \rangle h(\tau') \, d\tau' \tag{43}$$

and

$$z(\tau) \equiv \exp\left\{ -\int_{\tau_{1/2}}^{\tau} S_\omega(\tau') \, d\tau' \right\}. \tag{44}$$

From Eqs. (41)–(44) we obtain

$$\begin{aligned} d\Omega(\tau) &= (d\omega^*(\tau) - \Omega \, dz(\tau) - dg(\tau))/z \\ &= -(g/z) S_\omega \, d\tau - C_\chi \left(\Omega + \frac{g}{z} \right) d\tau \\ &\quad \left[\ln\left(\frac{\Omega z + g}{\langle\omega\rangle} \right) - \mathcal{L} \right] \\ &\quad + (2C_\chi \sigma^2)^{1/2} \left(\Omega + \frac{g}{z} \right) dW_\tau(\tau). \end{aligned} \tag{45}$$

The first approximation is now made: in order to obtain $\Omega(\bar{\tau}) - \Omega(0)$, Eq. (45) is integrated from $\tau = 0$ to $\tau = \bar{\tau}$ with the coefficients frozen at their mid-time values. Since $g(\tau_{1/2}) = 0$ and $z(\tau_{1/2}) = 1$, with frozen coefficients, Eq. (45) becomes

$$\begin{aligned} d\Omega(\tau) = &-C_\chi \Omega \, d\tau \left[\ln\left(\frac{\Omega}{\langle\omega\rangle_{1/2}} \right) - \mathcal{L}_{1/2} \right] \\ &+ (2C_\chi \sigma^2)^{1/2} \Omega \, dW_\tau(\tau), \end{aligned} \tag{46}$$

where the constant coefficients $\langle\omega\rangle_{1/2}$ and $\mathcal{L}_{1/2}$ are estimates for $\langle\omega\rangle$ and $\mathcal{L}$ at $\tau_{1/2}$. On the predictor and corrector steps, $\langle\omega\rangle_{1/2}$ is approximated by

$$\begin{aligned} \langle\omega\rangle_{1/2} &= \langle\omega^*(t_j)\rangle_N \qquad \text{(predictor)} \\ &= \tfrac{1}{2}[\langle\omega^*(t_j)\rangle_N + \langle\hat{\omega}(t_{j+1})\rangle_N] \qquad \text{(corrector)} \end{aligned} \tag{47}$$

and similarly for $\mathcal{L}_{1/2}$.

The final transformation is to define

$$\chi(\tau) = \ln[\Omega(\tau)/\Omega(0)]. \tag{48}$$

Then from Eq. (46) we obtain

$$d\chi(\tau) = -C_\chi \, d\tau [\chi - \chi_\infty] + (2C_\chi \sigma^2)^{1/2} \, dW_\tau(\tau), \tag{49}$$

where

$$\chi_\infty \equiv \mathcal{L}_{1/2} - \sigma^2 - \ln\left(\frac{\Omega(0)}{\langle\omega\rangle_{1/2}} \right). \tag{50}$$

Equation (49) is the strictly linear stochastic differential equation [38] corresponding to $\chi(\tau)$ being an OU process (with initial condition $\chi(0) = 0$). At time $\bar{\tau}$ the exact solution $\chi(\bar{\tau})$ is a Gaussian random variable which can be written

$$\chi(\bar{\tau}) = \chi_\infty [1 - e^{-c_\chi \bar{\tau}}] + \xi\sigma [1 - e^{-2c_\chi \bar{\tau}}]^{1/2}, \tag{51}$$

where ξ is a standardized Gaussian random variable ($\langle\xi\rangle = 0$, $\langle\xi^2\rangle = 1$).

This completes the major steps in the solution for ω^*. It remains to unravel the transformations in order to obtain an explicit expression for $\omega^*(t_{j+1})$, and to provide some detailed specifications.

From Eqs. (42) and (48) we obtain

$$\omega^*(\bar{\tau}) = z(\bar{\tau}) \Omega(0) \exp(\chi(\bar{\tau})) + g(\bar{\tau}) \tag{52}$$

and

$$\Omega(0) = (\omega^*(0) - g(0))/z(0). \tag{53}$$

The remaining quantities to be determined are integrals over the time interval. These are approximated using the coefficients frozen at $\tau_{1/2}$. Thus the approximations are

$$\bar{\tau} = \langle\omega\rangle_{1/2} \, \Delta t, \tag{54}$$

$$g(\bar{\tau}) = -g(0) = \langle\omega\rangle_{1/2} h_{1/2} \tau_{1/2}, \tag{55}$$

and

$$z(\bar{\tau}) = 1/z(0) = \exp(-S_{\omega 1/2}\tau_{1/2}), \tag{56}$$

where $h_{1/2}$ and $S_{\omega 1/2}$ are evaluated similarly to $\langle\omega\rangle_{1/2}$ in Eq. (45).

The final result for $\omega^*(t_{j+1})$ (or $\hat{\omega}(t_{j+1})$) can now be written

$$\begin{aligned}\omega^*(t_{j+1}) = \omega_h \exp\Bigg\{ & -\bar{\tau}S_{\omega 1/2} \\ & + [1 - e^{-C_\chi \bar{\tau}}]\Bigg[\frac{\mathscr{L}_{1/2} - \sigma^2}{} \\ & + \frac{1}{2}\bar{\tau}S_{\omega 1/2} - \ln\left(\frac{\omega_h}{\langle\omega\rangle_{1/2}}\right)\Bigg] \\ & + \xi\sigma[1 - e^{-2C_\chi\bar{\tau}}]^{1/2}\Bigg\} + \frac{1}{2}\bar{\tau}\langle\omega\rangle_{1/2}h_{1/2},\end{aligned} \tag{57}$$

where

$$\omega_h = \omega^*(t_j) + \tfrac{1}{2}\bar{\tau}\langle\omega\rangle_{1/2}h_{1/2}. \tag{58}$$

On both predictor and corrector steps, once Eq. (57) has been used to determine $\omega^{(n)}(t_{j+1})$ (or $\hat{\omega}^{(n)}(t_{j+1})$), a small variance-reduction correction is made to remove the randomness in $\langle\omega(t_{j+1})\rangle_N$ caused by the random variables ξ. This correction is based on a numerical solution of the exact equation for $\langle\omega\rangle$:

$$\frac{d}{dt}\langle\omega\rangle = -\langle\omega\rangle^2(S_\omega + h). \tag{59}$$

Using a procedure similar to that for ω^*, an approximate solution for $\langle\omega(t_{j+1})\rangle$ is

$$\langle\omega(t_{j+1})\rangle = \langle\omega_h\rangle_N \exp(-\bar{\tau}S_{\omega 1/2}) + \tfrac{1}{2}\bar{\tau}\langle\omega\rangle_{1/2}h_{1/2}. \tag{60}$$

Thus the variance reduction technique is simply to apply the same multiplicative correction to each particle frequency $\omega^{(n)}(t_{j+1})$ so that, after adjustment, the ensemble mean $\langle\omega(t_{j+1})\rangle_N$ equals the mean given by Eq. (60).

The following are clarifications and comments on the above method:

1. In a more explicit notation, let $\xi_j^{(n)}$ be the standardized Gaussian random variable used in Eq. (57) for the nth particle on the jth step. These are all independent (i.e., $\langle\xi_j^{(n)}\xi_k^{(m)}\rangle = \delta_{nm}\,\delta_{jk}$). However, the same value of $\xi_j^{(n)}$ is used on the predictor and corrector steps.

2. In the degenerate case $\langle\omega\rangle_N = 0$, the exact solution $\omega^{(n)}(t_{j+1}) = 0$ should be used, to avoid division by zero and other difficulties.

3. An important special case is when some (but not all) of the particles have zero frequency, $\omega^{(n)}(t_j) = 0$ (some n). In these circumstances, it is the intention of the model for h to be strictly positive. An analysis of the sde shows that the leading order terms in an expansion for $\omega^{(n)}(t)$ are of order τ and $\tau^2 \ln \tau$. The numerical solution matches the expansion to this order. If (contrary to the intention of the model) h is zero, then Eq. (57) remains valid (since ω_h (which is zero) appears as $\omega_h \ln \omega_h$) and yields the correct result: $\omega^{(n)}(t_{j+1}) = 0$.

4. In deriving the expression for $\omega^*(t_{j+1})$, Eq. (57), the only approximation made is to replace the coefficients with their mid-time values. This has two consequences. First, if the coefficients were constant, then the solution would be exact for arbitrarily large Δt. Second, for the general case of time-dependent coefficients, the use of mid-time values ensures that the scheme is second-order accurate in time. (On the predictor and corrector steps, $\langle\omega\rangle_{1/2}$, Eq. (47), provides first-order and second-order accurate approximations to $\langle\omega(\tau_{1/2})\rangle$, respectively.)

5. It may be observed that the predictor $\hat{\omega}(t_{j+1})$ is not used in the corrector step, except to evaluate the coefficients.

6. The simple variance-reduction techniques used remove all randomness in $\langle\omega\rangle$, except for that entering through the coefficient h.

5. NUMERICAL INTEGRATION OF VELOCITY

At the general time level $t_j = j\,\Delta t$, the task is to integrate the stochastic differential equation (Eq. (21)) for the velocity $\mathbf{u}^*(t)$ of the general particle in order to obtain $\mathbf{u}^*(t_{j+1})$.

In this section it proves convenient to use matrix notation (more than tensor notation). So the stochastic differential equation for $\mathbf{u}^*(t)$ (Eq. (21)) is rewritten

$$\begin{aligned}d\mathbf{u}^*(t) = & -\boldsymbol{\Gamma}\mathbf{u}^*\,dt + \mathbf{D}(\mathbf{u}^*, \omega^*, t)\,dt \\ & + (C_0\tilde{k}\omega^*)^{1/2}\,d\mathbf{W}(t).\end{aligned} \tag{61}$$

5.1. *Mean Velocity Gradients*

The term in the mean velocity gradients $\boldsymbol{\Gamma}$ is the same general form as the drift term $\mathbf{D}$, and, hence, the two terms could be treated together. However, with extensions to inhomogenous flows in mind, a decomposition is used to separate the two processes.

The particle velocity is decomposed as

$$\mathbf{u}^*(t) = \boldsymbol{\gamma}(t) + \mathbf{z}(t), \tag{62}$$

with

$$\frac{d\boldsymbol{\gamma}}{dt} = -\boldsymbol{\Gamma}\mathbf{u}^*, \tag{63}$$

and

$$d\mathbf{z}(t) = \mathbf{D}(\mathbf{u}^*, \omega^*, t)\,dt + (C_0\tilde{k}\omega^*)^{1/2}\,d\mathbf{W}(t). \tag{64}$$

At the beginning of the time step (t_j), the initial condition for $\boldsymbol{\gamma}$ is specified as

$$\boldsymbol{\gamma}(t_j) = \tfrac{1}{2}\boldsymbol{\Gamma}(t_j)\mathbf{u}^*(t_j)\,\Delta t, \tag{65}$$

and, hence, the initial condition for $\mathbf{z}$ is

$$\mathbf{z}(t_j) = \mathbf{u}^*(t_j) - \tfrac{1}{2}\boldsymbol{\Gamma}(t_j)\mathbf{u}^*(t_j)\,\Delta t. \tag{66}$$

At the end of the time step, when $\mathbf{z}(t_{j+1})$ has been determined, Eq. (63) is integrated by the trapezoidal method to yield the implicit equation

$$\boldsymbol{\gamma}(t_{j+1}) = -\tfrac{1}{2}\boldsymbol{\Gamma}(t_{j+1})\mathbf{u}^*(t_{j+1})\,\Delta t, \tag{67}$$

or, explicitly,

$$[\mathbf{I} + \tfrac{1}{2}\boldsymbol{\Gamma}(t_{j+1})\,\Delta t]\boldsymbol{\gamma}(t_{j+1}) = -\tfrac{1}{2}\boldsymbol{\Gamma}(t_{j+1})\mathbf{z}(t_{j+1})\,\Delta t, \tag{68}$$

where $\mathbf{I}$ is the 3×3 identity matrix.

The initial condition for $\boldsymbol{\gamma}$ is chosen so that (to a good approximation) $\boldsymbol{\gamma}$ is zero at the mid-time $t_{j+1/2} = \frac{1}{2}(t_j + t_{j+1})$. For given $\mathbf{u}^*(t_j)$, $\boldsymbol{\gamma}(t)$ is a differentiable random function that is of order Δt, in the interval $[t_j, t_{j+1}]$. At the mid-time, the mean of $\boldsymbol{\gamma}(t_{j+1/2})$ is of order Δt^2, and its variance is of order Δt^3.

The value of $\mathbf{z}$ at t_{j+1} is obtained by integrating Eq. (64) from t_j to t_{j+1}. First substituting $\mathbf{z} + \boldsymbol{\gamma}$ for $\mathbf{u}^*$, we obtain

$$\begin{aligned}\mathbf{z}(t_{j+1}) - \mathbf{z}(t_j) = &\int_{t_j}^{t_{j+1}} \mathbf{D}(\mathbf{z}[t'] + \boldsymbol{\gamma}[t'], \omega^*[t'], t')\,dt' \\ &+ \int_{t_j}^{t_{j+1}} (C_0\tilde{k}[t']\omega^*[t'])^{1/2}\,d\mathbf{W}(t').\end{aligned} \tag{69}$$

The integral of $\mathbf{D}$ is evaluated by replacing $\boldsymbol{\gamma}(t')$ by its mid-time value $\boldsymbol{\gamma}(t_{j+1/2})$—which is zero (to a good approximation). Then Eq. (69) corresponds to the solution of the stochastic differential equation

$$d\mathbf{z}(t) = \mathbf{D}(\mathbf{z}, \omega^*, t) + (C_0\tilde{k}\omega^*)^{1/2}\,d\mathbf{W}(t). \tag{70}$$

In summary, for each time step, $\mathbf{u}^*(t)$ is decomposed into an order $-\Delta t$ increment $\boldsymbol{\gamma}(t)$ arising from the mean velocity gradients, and a stochastic component $\mathbf{z}(t)$. From the given initial condition (Eq. (66)), $\mathbf{z}(t_{j+1})$ is determined from Eq. (70)—which is independent of $\boldsymbol{\gamma}(t)$. Then $\boldsymbol{\gamma}(t_{j+1})$ is obtained from Eq. (68).

5.2. *Separation of Frequency Dependent Components*

The task now is to integrate the stochastic differential equation for $\mathbf{z}(t)$ in Eq. (70). It is essential to the approach to obtain a stable, accurate solution to this equation, even if $\omega^*\,\Delta t$ is not small compared to unity. This is achieved by separating the ω^*-dependent terms and transforming the resulting equation to a strictly linear stochastic differential equation, which has an analytic solution.

The drift coefficient (Eq. (23)) can be decomposed as

$$\mathbf{D}(\mathbf{z}, \omega^*, t) = -\omega^*\mathbf{B}\mathbf{z} + \mathbf{D}^0(\mathbf{z}, t), \tag{71}$$

where $\mathbf{D}^0$ is independent of ω^* and $\mathbf{B}$ is the symmetric positive-definite 3×3 matrix

$$\mathbf{B} = \tfrac{3}{4}C_0\tilde{\mathbf{A}}^{-1}. \tag{72}$$

Then $\mathbf{z}(t)$ can be decomposed into a stochastic ω^*-dependent part $\mathbf{R}(t)$ and an order-Δt, differentiable, ω^*-independent part $\mathbf{V}(t)$ as follows:

$$\mathbf{z}(t) = \mathbf{R}(t) + \mathbf{V}(t), \tag{73}$$

$$\mathbf{R}(t_j) = \mathbf{z}(t_j), \quad \mathbf{V}(t_j) = 0, \tag{74}$$

$$d\mathbf{R}(t) = -\omega^*\mathbf{B}(\mathbf{R} + \mathbf{V})\,dt + (C_0\tilde{k}\omega^*)^{1/2}\,d\mathbf{W}(t), \tag{75}$$

$$\frac{d\mathbf{V}(t)}{dt} = \mathbf{D}^0(\mathbf{R} + \mathbf{V}, t). \tag{76}$$

5.3. *Solution for R*

The equation for $\mathbf{R}$ is simplified by introducing the particle-dependent normalized time $\tau(t)$:

$$\tau(t) = \int_{t_j}^{t} \omega^*(t')\,dt'. \tag{77}$$

(Note that this is different from the normalized time τ defined in Section 4 for the ω^* equation.) As before, the start of the time step is $\tau(t_j) = 0$, and the end is denoted by $\bar{\tau} = \tau(t_{j+1})$. With all variables expressed as functions of τ, Eq. (75) transforms to

$$d\mathbf{R}(\tau) = -\mathbf{B}(\mathbf{R} + \mathbf{V})\,d\tau + (C_0\tilde{k})^{1/2}\,d\mathbf{w}(\tau), \tag{78}$$

where the increments of the Wiener process $\mathbf{w}(\tau)$ have the covariance matrix

$$\langle d\mathbf{w}(d\mathbf{w})^{\mathrm{T}}\rangle = d\tau\,\mathbf{I} = \omega^*\,dt\,\mathbf{I}. \tag{79}$$

On the predictor step the coefficients $\mathbf{B}$ and $\tilde{k}$ are frozen at their ensemble averaged values at t_j and $\bar{\tau}$ is approximated as $\omega^*(t_j)\,\Delta t$. On the corrector step, the coefficients are frozen at the average of their ensemble averaged values at t_j and t_{j+1} (based on predictor particle properties), and $\bar{\tau}$ is approximated as $\frac{1}{2}(\omega^*(t_j) + \hat{\omega}(t_{j+1}))\,\Delta t$.

We recall that $\mathbf{V}(\tau)$ is of order Δt, is differentiable, and is zero at the beginning of the step. Consequently, on the corrector step (for $\mathbf{R}$), a good approximation is

$$\mathbf{V}(\tau) = \hat{\mathbf{V}}\tau/\bar{\tau}, \tag{80}$$

where $\hat{\mathbf{V}}$ is the predictor for $\mathbf{V}(\bar{\tau})$ (or $\mathbf{V}(t_{j+1})$).

On the predictor step (for $\mathbf{R}$), $\mathbf{V}(\tau) = 0$ is an adequate approximation, which (in order to unify the notation) we implement by defining $\hat{\mathbf{V}} = 0$ on the predictor step.

With these specifications Eq. (78) becomes

$$d\mathbf{R}(\tau) = -\mathbf{B}(\mathbf{R} + \hat{\mathbf{V}}\tau/\bar{\tau})\, d\tau + (C_0\tilde{k})^{1/2}\, d\mathbf{w}(\tau) \tag{81}$$

with $\mathbf{B}$, $\hat{\mathbf{V}}$, and $\tilde{k}$ being frozen coefficients.

This coupled set of three stochastic differential equations is decoupled by transforming to the principal axes of $\mathbf{B}$. Since $\mathbf{B}$ is symmetric positive definite, it can be expressed as

$$\mathbf{B} = \mathbf{Q}\boldsymbol{\Lambda}\mathbf{Q}^{\mathrm{T}}, \tag{82}$$

where $\mathbf{Q}$ is the real unitary matrix and $\boldsymbol{\Lambda}$ is the diagonal matrix of real positive eigenvalues λ_1, λ_2, and λ_3. Thus, defining

$$\mathbf{r}(\tau) = \mathbf{Q}^{\mathrm{T}}\mathbf{R}(\tau) \tag{83}$$

and

$$\hat{\mathbf{v}} = \mathbf{Q}^{\mathrm{T}}\hat{\mathbf{V}}, \tag{84}$$

and premultiplying Eq. (81) by $\mathbf{Q}^{\mathrm{T}}$, we obtain

$$d\mathbf{r}(\tau) = -\boldsymbol{\Lambda}(\mathbf{r} + \hat{\mathbf{v}}\tau/\bar{\tau})\, d\tau + (C_0\tilde{k})^{1/2}\, d\mathbf{w}(\tau). \tag{85}$$

(The same symbol is used for the Wiener process, since it is statistically invariant under unitary transformations.) Since $\boldsymbol{\Lambda}$ is diagonal, Eq. (85) consists of three independent equations for $r_1(\tau)$, $r_2(\tau)$, and $r_3(\tau)$. Omitting the suffices, each of these scalar equations is

$$dr(\tau) = -\lambda(r + \hat{v}\tau/\bar{\tau})\, d\tau + (C_0\tilde{k})^{1/2}\, dw(\tau). \tag{86}$$

This equation is solved by observing that the quantity

$$\rho(\tau) \equiv r(\tau) + \frac{\hat{v}\tau}{\bar{\tau}} - \frac{\hat{v}}{\lambda\bar{\tau}} \tag{87}$$

is an OU process satisfying

$$d\rho(\tau) = -\lambda\rho(\tau)\, d\tau + (C_0\tilde{k})^{1/2}\, dw(\tau). \tag{88}$$

The exact solution to this equation is

$$\rho(\bar{\tau}) = \rho(0)e^{-\lambda\bar{\tau}} + \xi\left[\frac{C_0\tilde{k}}{2\lambda}(1 - e^{-2\lambda\bar{\tau}})\right]^{1/2}, \tag{89}$$

where ξ is a standardized Gaussian random variable. Hence the solution for $r(\bar{\tau})$ is

$$r(\bar{\tau}) = r(0)e^{-\lambda\bar{\tau}} - \hat{v}\left(1 - \frac{1 - e^{-\lambda\bar{\tau}}}{\lambda\bar{\tau}}\right) + \xi\left[\frac{C_0\tilde{k}}{2\lambda}(1 - e^{-2\lambda\bar{\tau}})\right]^{1/2}. \tag{90}$$

From the above solution for all three components of $\mathbf{r}(\bar{\tau})$, the solution $\mathbf{R}(\bar{\tau})$ is obtained by transforming back to the original coordinates:

$$\mathbf{R}(\bar{\tau}) = \mathbf{Q}\mathbf{r}(\bar{\tau}). \tag{91}$$

(A detail of some practical importance is the computational evaluation of the exponential terms in Eq. (90); with $x = \lambda\bar{\tau}$, these are $E_1(x) \equiv e^{-x}$, $E_2(x) \equiv 1 - (1 - E_1(x))/x$, and $E_3(x) \equiv (1 - E_2(x)^2)^{1/2}$. Apart from the expense of computing exponentials, the direct evaluation of E_2 (and to a lesser extent E_3) is ill-conditioned. Instead, for $E_1(x)$ we use the rational approximation

$$E_1(x) = \frac{1 - \frac{1}{3}x}{1 + \frac{2}{3}x + \frac{1}{6}x^2}, \tag{92}$$

from which similar approximations for E_2 and E_3 are obtained. The formal order of accuracy provided by these approximations is better than second order. For all x, the errors in $E_2(x)$ and $E_3(x)$ are less than 2% and $\frac{1}{2}$%, respectively. The error in $E_1(x)$ is less than 1% for $x < 1.3$, but peaks at 10% at $x = 8$.)

5.4. *Solution for* $\boldsymbol{V}$

A straightforward predictor–corrector is used to solve Eq. (76) for $\mathbf{V}(t_{j+1})$. The predictor is

$$\hat{\mathbf{V}} = \Delta t\, \mathbf{D}^0(\mathbf{R}(t_j), t_j), \tag{93}$$

and the corrector is

$$\mathbf{V}(t_{j+1}) = \Delta t\, \mathbf{D}^0(\mathbf{z}_{1/2}, t_{1/2}), \tag{94}$$

where

$$\mathbf{z}_{1/2} \equiv \tfrac{1}{2}[\mathbf{R}(t_j) + \mathbf{R}(t_{j+1}) + \hat{\mathbf{V}}]. \tag{95}$$

This completes the solution. The final result is

$$\mathbf{u}^*(t_{j+1}) = \boldsymbol{\gamma}(t_{j+1}) + \mathbf{R}(t_{j+1}) + \mathbf{V}(t_{j+1}), \tag{96}$$

where the three contributions on the right-hand side are given by Eqs. (68), (91), and (94).

5.5. *Variance Reduction*

At the end of the predictor and corrector steps, the ensemble average mean $\langle \mathbf{z} \rangle_N$ and covariance $\langle z_i z_j \rangle_N$ contain statistical errors arising from the Gaussian random variables $\boldsymbol{\xi} = \{\xi_1, \xi_2, \xi_3\}$ used in Eq. (90). By definition, the *primary* random contribution scales as $\boldsymbol{\xi}\, \Delta t^{1/2}$, whereas *secondary* contributions scale as $\boldsymbol{\xi}\, \Delta t^{3/2}$. An expansion of the exponential in Eq. (90) reveals that the primary random contribution to $\mathbf{R}(\bar{\tau})$ is

$$\mathbf{P} = \boldsymbol{\xi}(C_0 \tilde{k} \omega^* \, \Delta t)^{1/2}. \tag{97}$$

Secondary contributions stem both from higher-order terms in this expansion and from the dependence of $\mathbf{V}(t_{j+1})$ on $\mathbf{R}(t_{j+1})$ (Eqs. (94) and (95)).

In this section a variance-reduction technique is described which completely removes the primary statistical errors in $\langle \mathbf{z} \rangle_N$ and $\langle z_i z_j \rangle_N$—that is, the errors arising from $\mathbf{P}$. The central idea is to compute estimates of $\langle \mathbf{z} \rangle$ and $\langle z_i z_j \rangle$ (denoted by $\langle \mathbf{z} \rangle_{4N}$ and $\langle z_i z_j \rangle_{4N}$) that are free of primary statistical error. Then, as with the initial conditions (Eqs. (36), (38)) the particle velocities are corrected to

$$\bar{\mathbf{z}}^{(n)} = (\mathbf{I} + \mathbf{L})(\mathbf{z}^{(n)} + \mathbf{z}^0), \tag{98}$$

where the vector $\mathbf{z}^0$ and the lower triangular matrix $\mathbf{L}$ are uniquely determined by the conditions that $\langle \bar{\mathbf{z}} \rangle_N$ and $\langle \bar{z}_i \bar{z}_j \rangle_N$ equal $\langle \mathbf{z} \rangle_{4N}$ and $\langle z_i z_j \rangle_{4N}$. This correction is simple to perform; the issue is the determination of the statistical-error-free estimates $\langle \mathbf{z} \rangle_{4N}$ and $\langle z_i z_j \rangle_{4N}$.

To a first approximation, the statistical error arises because $\langle \boldsymbol{\xi} \rangle_N$ is not identically zero and because $\langle \xi_i \xi_j \rangle_N$ is not identically δ_{ij}.

Consider then, instead, the set of $4N$ random vectors denoted by $\boldsymbol{\eta}^{(n,\alpha)}$ ($n = 1, 2, \ldots, N$; $\alpha = 1, 2, 3, 4$), defined geometrically as follows: Each vector $\boldsymbol{\eta}^{(n,\alpha)}$ is on the sphere of radius $\sqrt{3}$, centered at the origin. For each n, the four vectors $\boldsymbol{\eta}^{(n,\alpha)}$ ($\alpha = 1, 2, 3, 4$) form the vertices of a regular tetrahedron. The orientations of the tetrahedra are random, uniformly distributed, and independent for each n.

Since $\boldsymbol{\eta}^{(n,\alpha)}$ is an isotropic random vector of length $\sqrt{3}$, it follows that

$$\langle \boldsymbol{\eta}^{(n,\alpha)} \rangle = 0, \quad \langle \eta_i^{(n,\alpha)} \eta_j^{(n,\alpha)} \rangle = \delta_{ij}. \tag{99}$$

But most importantly, from the geometry of the tetrahedron, we have

$$\frac{1}{4} \sum_{\alpha=1}^{4} \boldsymbol{\eta}^{(n,\alpha)} = 0 \tag{100}$$

and

$$\frac{1}{4} \sum_{\alpha=1}^{4} \eta_i^{(n,\alpha)} \eta_j^{(n,\alpha)} = \delta_{ij}. \tag{101}$$

That is, averaged over the four samples, the first and second moments of $\boldsymbol{\eta}^{(n,\alpha)}$ contain no randomness.

Using the numerical method described earlier in this section, for each of the N particles, starting from the initial condition $\mathbf{z}^{(n)}(t_j)$, four estimates $\mathbf{z}^{(n,\alpha)}(t_{j+1})$ ($\alpha = 1, 2, 3, 4$) of $\mathbf{z}^{(n)}(t_{j+1})$ are obtained by replacing $\boldsymbol{\xi}$ by $\boldsymbol{\eta}^{(n,\alpha)}$ in Eq. (90). Then $\langle \mathbf{z} \rangle_{4N}$ is defined by

$$\langle \mathbf{z} \rangle_{4N} = \frac{1}{4N} \sum_{n=1}^{N} \sum_{\alpha=1}^{4} \mathbf{z}^{(n,\alpha)}(t_{j+1}) \tag{102}$$

and similarly for $\langle z_i z_j \rangle_{4N}$.

The primary statistical error in $\langle \mathbf{z} \rangle_{4N}$ is

$$\langle \mathbf{P} \rangle_{4N} - \langle \mathbf{P} \rangle = \frac{1}{4N} \sum_{n=1}^{N} \sum_{\alpha=1}^{4} \boldsymbol{\eta}^{(n,\alpha)} (C_0 \tilde{k} \omega^{(n)} \, \Delta t)^{1/2}, \tag{103}$$

which is zero because of Eq. (100). The corresponding error in $\langle z_i z_j \rangle_{4N}$ is

$$\begin{aligned} \langle P_i P_j \rangle_{4N} - \langle P_i P_j \rangle = \frac{1}{4N} \sum_{n=1}^{N} \sum_{\alpha=1}^{4} \eta_i^{(n,\alpha)} \eta_j^{(n,\alpha)} C_0 \tilde{k} \omega^{(n)} \, \Delta t \\ - \delta_{ij} C_0 \tilde{k} \langle \omega \rangle_N \, \Delta t, \end{aligned} \tag{104}$$

which again is zero, in view of Eq. (101).

To summarize the variance-reduction method: using the tetrahedral random vectors $\boldsymbol{\eta}^{(n,\alpha)}$, $4N$ samples $\mathbf{z}^{(n,\alpha)}(t_{j+1})$ of $\mathbf{z}(t_{t+1})$ are obtained. The ensemble average mean $\langle \mathbf{z} \rangle_{4N}$ and covariance $\langle z_i z_j \rangle_{4N}$ of these samples are free of primary statistical error. The values of $\mathbf{z}^{(n)}(t_{j+1})$ obtained with the Gaussian random vectors $\boldsymbol{\xi}^{(n)}$ are then corrected (Eq. (98)) so that their ensemble mean and covariance equal $\langle \mathbf{z} \rangle_{4N}$ and $\langle z_i z_j \rangle_{4N}$.

This procedure is applied after both predictor and corrector steps. There is, of course, a computational cost to pay: For each particle five estimates of $\mathbf{z}(t_{j+1})$ must be generated (i.e., $\mathbf{z}^{(n)}(t_{j+1})$, based on $\boldsymbol{\xi}^{(n)}$, and $\mathbf{z}^{(n,\alpha)}(t_{j+1})$, based on $\boldsymbol{\eta}^{(n,\alpha)}$, $\alpha = 1, 2, 3, 4$). But, as the results of the next section show, the benefit far outweighs the cost. (A small computational saving stems from the observation that, on the predictor step only, $\boldsymbol{\xi}^{(n)}$ does not need to be Gaussian. Thus $\mathbf{z}^{(n,1)}(t_{j+1})$, say, can be used for $\mathbf{z}^{(n)}(t_{j+1})$, reducing the required number of estimates to four.)

6. RESULTS

In order to examine the convergence, accuracy, and efficiency of the numerical method, in this section results are reported for two cases. The first test case, which is examined in the

most detail, is of sheared Gaussian homogeneous turbulence. An exact analytic solution is available, which greatly facilitates precise testing. However, aspects of the numerical method—particularly the treatment of particles with zero frequency—are not tested in this flow. Consequently, a second test case with a bimodal turbulent/non-turbulent initial condition is also examined (Section 6.5).

6.1. *Sheared Gaussian Homogeneous Turbulence*

For the class of homogeneous turbulent flows considered, a particular flow is completely defined by the initial joint pdf of $\mathbf{u}$ and ω, $f(\mathbf{v}, \theta; 0)$, and by the mean velocity-gradient tensor $\Gamma_{ij}(t)$, Eq. (4). For the first test case described in this subsection, the initial condition is that $u_1(0)$, $u_2(0)$, $u_3(0)$ and $\ln(\omega(0)/\langle\omega(0)\rangle)$ are joint-normally distributed with unit covariance matrix. The means are $\langle\mathbf{u}(0)\rangle = 0$ and $\langle\omega(0)\rangle = 1$. Thus the initial joint pdf is

$$f(\mathbf{v}, \theta; 0) = \frac{1}{4\pi^2\theta}\exp\left\{-\frac{1}{2}\mathbf{v}\cdot\mathbf{v} - \frac{1}{2}\ln\theta - \frac{1}{4}\right\}. \quad (105)$$

Corresponding to simple shear, all the components of the velocity gradient tensor are zero except for

$$\Gamma_{12}(t) = \frac{\partial\langle U_1\rangle}{\partial x_2}. \quad (106)$$

The specification of $\Gamma_{12}(t)$ is contrived so that a relatively simple analytic solution can be obtained. The implicit specification is

$$\Gamma_{12}(t) = \Gamma_0\langle\omega(t)\rangle, \quad (107)$$

where

$$\Gamma_0 = (1 + \tfrac{3}{2}C_0)/\sqrt{C_0} \approx 3.34, \quad (108)$$

and $C_0 = 3.5$ is a model constant.

The model equations are constructed so that in Gaussian homogeneous turbulence (as here) $\mathbf{u}^*(t)$ and $\ln\omega^*(t)$ remain joint normal, with $\mathbf{u}^*(t)$ being independent of $\omega^*(t)$ [12, 13]. Furthermore, $\langle\mathbf{u}(t)\rangle$ remains zero and the variance of $\ln\omega^*(t)$ remains equal to $\sigma^2 = 1$. Thus the joint pdf is completely determined by the mean frequency $\langle\omega(t)\rangle$ and by the Reynolds stresses $\langle u_i u_j\rangle$. The evolution equations for $\langle\omega(t)\rangle$ (obtained from Eq. (14)) and for $\langle u_i u_j\rangle$ (obtained from Eq. (21)) then form a closed set. From the given initial conditions, the analytic solution to these equations is given in Appendix A.

(The analytic solution is obtained using the true inverses of $\mathbf{A}$ and $\tilde{\mathbf{A}}$, rather than the modified-determinant inverses. Consequently (for this test case only) the true inverses were used in the numerical method also, so that the numerical solution should indeed converge to the analytic solution.)

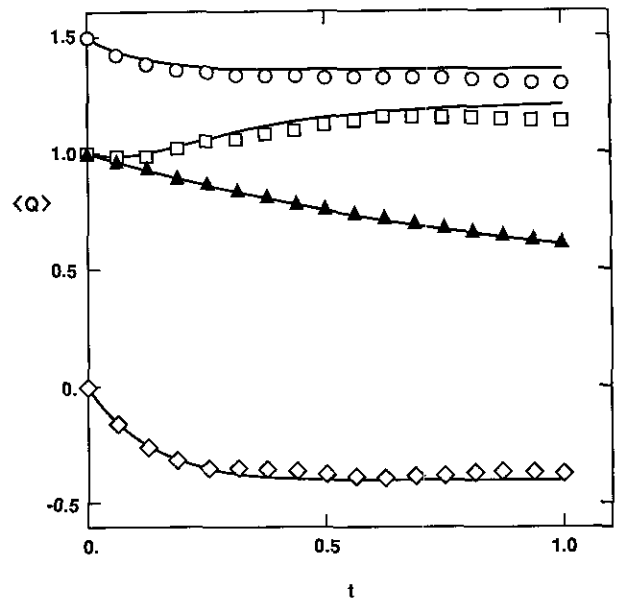

FIG. 1. Temporal evolution of statistics for the homogeneous shear test case. Solid lines—exact solution; symbols—numerical solution ($N = 256$, $\Delta t = \frac{1}{16}$): ○, k; □, $\langle u_1^2\rangle$; ◇, $\langle u_1 u_2\rangle$; △, $\langle\omega\rangle$.

In the tests to be described the statistics monitored are: k, $\langle u_1^2\rangle$, $\langle u_1 u_2\rangle$, $K \equiv \langle u_1^4\rangle/\langle u_1^2\rangle^2$, $\langle\omega\rangle$, $\mu_{1/2} \equiv \langle(\omega/\langle\omega\rangle)^{1/2}\rangle$, and $\tilde{k}/k$. The first four involve only $\mathbf{u}$, the next two only ω, while $\tilde{k}/k$ depends on both $\mathbf{u}$ and ω. The moments k, $\langle u_1^2\rangle$, $\langle u_1 u_2\rangle$, and $\langle\omega\rangle$ are "controlled" by the variance reduction schemes, while the remainder are not. The analytic solution for these moments is given in Appendix A, while the values of the other statistics are determined from the known joint-normality of $\mathbf{u}$ and ω:

$$\mu_{1/2} = e^{-\sigma^2/8}, \quad K = 3, \quad \tilde{k}/k = 1. \quad (109)$$

On Fig. 1, the exact solutions for k, $\langle u_1^2\rangle$, $\langle u_1 u_2\rangle$, and $\langle\omega\rangle$ (solid lines) are compared with ensemble average values, obtained from the numerical procedure with $N = 256$, $\Delta t = \frac{1}{16}$. As discussed in Section 3, the observed errors can be decomposed into three contributions (Eq. (32)): statistical error, bias, and time-stepping error. These three types of error are examined in the next three subsections.

6.2. *Statistical Error*

The statistical error in an ensemble average $\langle Q\rangle_N$ is measured by the standard error:

$$S_Q(t, N, \Delta t) = \sqrt{N\,\mathrm{var}(\langle Q\rangle_N)}. \quad (110)$$

Thus the root-mean-square statistical error is $N^{-1/2}S_Q$. By performing a large number M of independent trials, we can estimate the variance of $\langle Q\rangle_N$ and, hence, S_Q.

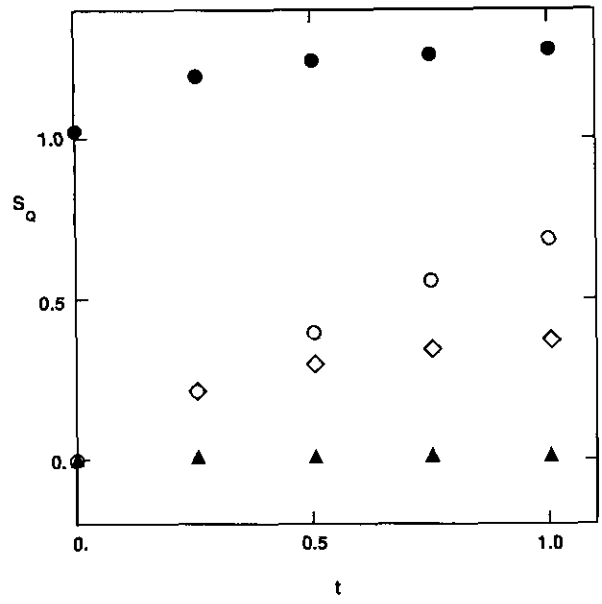

FIG. 2. Standard errors vs time: ○, k; ◇, $\langle u_1u_2\rangle$; △, $\langle\omega\rangle$; ●, $\tilde{k}/k$ (homogeneous shear, $N = 256$, $\Delta t = \frac{1}{16}$).

For $N = 256$ and $\Delta t = \frac{1}{16}$, Fig. 2 shows the standard errors in k, $\langle u_1u_2\rangle$, $\langle\omega\rangle$, and $\tilde{k}/k$ at different times, and their values at $t = 1$ are given in Table I. The error in $\langle\omega\rangle$ is extremely small ($S_\omega \approx 10^{-3}$). In the other controlled moments k, $\langle u_1^2\rangle$, and $\langle u_1u_2\rangle$, the error is initially zero and subsequently rises to modest values. For the uncontrolled quantities (K, $\mu_{1/2}$, and $\tilde{k}/k$) it varies little with time.

It is found that the standard errors are essentially independent of N: over the range investigated ($N = 128$–4096) S_Q varies by less than 10%. (An exception is S_ω which decreases weakly with N.) Similarly, varying Δt from $\frac{1}{16}$ to $\frac{1}{4}$ results, typically, in a 10–20% variation in S_Q.

The efficacy of the variance reduction techniques can be seen from Table I. Without the variance reduction on $\langle\omega\rangle$, the standard error S_ω increases a thousandfold (to $S_\omega^{(\omega)} = 1.2$). While without the variance reduction for $\langle u_iu_j\rangle$, their standard errors increase by a factor of 3 or 4. It may be observed, however, that the variance reduction techniques have essentially no effect on statistics other than those directly involved. Thus the standard errors in K, $\mu_{1/2}$, and $\tilde{k}/k$ are little affected.

The final row in Table I shows the relative CPU times, T, that are required. The variance reduction on $\langle\omega\rangle$ adds 1% to the time, while that on $\langle u_iu_j\rangle$ adds 20%. But, as is now shown, the benefit far outweighs this cost. The relative efficiency of different Monte Carlo implementations is determined by their *quality* [37], defined by

$$q = T'S_Q^2, \tag{111}$$

where T' is the CPU time required per particle. The smaller q is, the better. If N particles are used, the total CPU time required is $T = NT'$, and the variance in $\langle Q\rangle_N$ is S_Q^2/N. Hence, eliminating N, we obtain

$$\mathrm{var}(\langle Q\rangle_N) = T'S_Q^2/T, \tag{112}$$

or

$$T = q/\mathrm{var}(\langle Q\rangle_N). \tag{113}$$

In other words, the CPU time T required to achieve a specified statistical error level, $\mathrm{var}(\langle Q\rangle_N)$, is directly proportional to q. Taking $Q = u_1^2$, it may be seen from Table I that with variance reduction the quality (in arbitrary units) is $q = 1.21$, while without variance reduction it is $q^{(u,\omega)} = 3.2^2 = 10.24$. Thus, the use of variance reduction decreases the CPU time required by more than a factor of 8.

TABLE I

Standardized Errors for Different Variance-Reduction Techniques

$\langle Q\rangle$	S_Q	$S_Q^{(u)}/S_Q$	$S_Q^{(\omega)}/S_Q$	$S_Q^{(u,\omega)}/S_Q$
k	0.68	4.1	1.0	4.1
$\langle u_1^2\rangle$	0.81	3.2	1.0	3.2
$\langle u_1u_2\rangle$	0.37	3.3	1.0	3.3
K	4.85	1.0	1.0	1.0
$\langle\omega\rangle$	0.0012	1.1	1,000	1,000
$\mu_{1/2}$	0.22	1.0	1.0	1.0
$\tilde{k}/k$	1.28	1.1	1.0	1.1
$T/T^{(u,\omega)}$	1.21	1.01	1.21	1.00

Note. $t = 1$, $\Delta t = \frac{1}{16}$, $N = 256$; $S_Q^{(u,\omega)}$—no variance-reduction; $S_Q^{(\omega)}$—no variance-reduction on $\langle\omega\rangle$; $S_Q^{(u)}$—no variance-reduction on $\langle u_iu_j\rangle$; S_Q—both variance reductions used; T—CPU time required.

6.3. *Bias*

The bias B_Q in an ensemble-average statistic $\langle Q\rangle_N$ is the deterministic error caused by N being finite,

$$B_Q(t, N, \Delta t) = \langle\langle Q\rangle_N\rangle - \langle Q\rangle_\infty. \tag{114}$$

The sole source of bias is the statistical fluctuations in the coefficients in the stochastic differential equations. If, instead, the coefficients were non-random, independent of the particle properties, then at any time t, the computed particle properties $\mathbf{u}^{(n)}(t)$, $\omega^{(n)}(t)$ would be independent, identically distributed, and independent of N. It follows then that B_Q would be zero (since $\langle\langle Q\rangle_N\rangle = \langle Q\rangle$ in this hypothetical case).

A simple analysis suggests that B_Q scales as N^{-1}. Let c denote the value of a particular coefficient on a particular time step prior to t (when B_Q is to be estimated). Now since c is evaluated as an ensemble average over the particles it is itself a random variable. Thus we can write

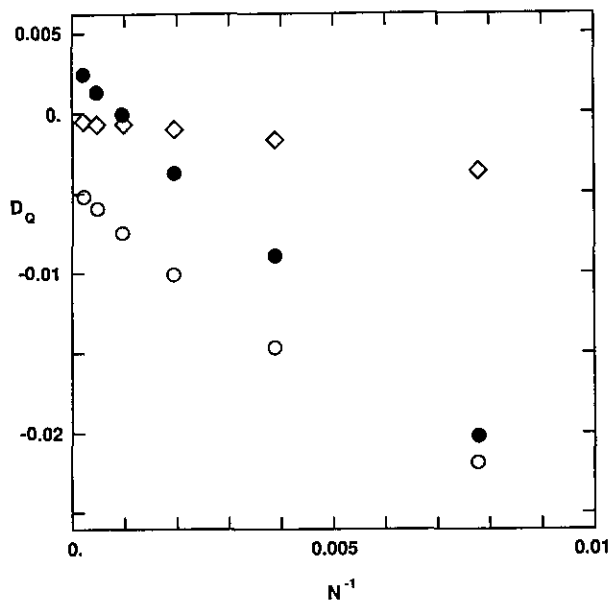

FIG. 3. Deterministic error vs N^{-1}: ○, k; ◇, $\langle u_2 u_2 \rangle$; ●, $\tilde{k}/k$ (homogeneous shear, $t = 1$, $\Delta t = \frac{1}{16}$).

$$c = c_0 + S_c N^{-1/2} \xi, \tag{115}$$

where ξ is a standardized random variable and (to a first approximation) c_0 and S_c are independent of N.

The dependence of $\langle Q \rangle_N$ (and hence of B_Q) on the value of c is expressed by the conditional expectation

$$q(\hat{c}) \equiv \langle \langle Q \rangle_N | c = \hat{c} \rangle. \tag{116}$$

The expectation $\langle \langle Q \rangle_N \rangle$ can then be written

$$\langle \langle Q \rangle_N \rangle = \langle q(c) \rangle \tag{117}$$

$$= \langle q(c_0 + S_c N^{-1/2} \xi) \rangle, \tag{118}$$

and, expanding about c_0, we obtain

$$\langle \langle Q \rangle_N \rangle = \langle q(c_0) \rangle + \tfrac{1}{2} \langle q''(c_0) \rangle S_c^2 N^{-1} + O(N^{-3/2}). \tag{119}$$

This analysis can be extended to consider every coefficient on every time step and hence to reach the conclusion that B_Q scales (to leading order) as N^{-1}.

In a simulation the bias cannot be measured directly. The direct measure is of the total deterministic error

$$D_Q(t, N, \Delta t) = \langle \langle Q \rangle_N \rangle - \langle Q \rangle = B_Q(t, N, \Delta t) + T_Q(t, \Delta t). \tag{120}$$

But since, by definition, the time-stepping error is independent of N, the N-dependence of B_Q can be studied through D_Q.

Figure 3 shows the total deterministic error D_Q plotted against N^{-1} for the statistics k, $\langle u_1 u_2 \rangle$, and $\tilde{k}/k$. The approximate linearity of the plots confirms the scaling of B_Q with N^{-1} suggested by the analysis.

This observed linear dependence is used to isolate B_Q. Using the values at $N = 1024$ and $N = 4096$, D_Q is linearly extrapolated in N^{-1} to $N^{-1} = 0$ (i.e., $N = \infty$) to produce an estimate of T_Q. Then B_Q is obtained from Eq. (120). Figure 4 shows NB_Q as a function of N for the same statistics as Fig. 3. Again, the approximate constancy of NB_Q as N varies by a factor of 16 confirms the scaling of B_Q with N^{-1}. For the other statistics (not shown), both $NB_{u_1^2}$ and NB_K are less than 2 (in magnitude) and exhibit variations with N of a similar level to those in Fig. 4. Both B_ω and $B_{\mu_{1/2}}$ exhibit remarkable linearity with N^{-1}, with values of $NB_\omega = 0.01$ and $NB_{\mu_{1/2}} = 0.28$.

6.4. *Time-Stepping Error*

Of the three types of numerical error, the time-stepping error is the most difficult to measure, since it requires the elimination of the other two. This was achieved by using a very large number of particles ($N = 2^{18} \approx 2.6 \times 10^4$) and averaging over (typically) $M = 128$ independent trials. As a result, the bias can be estimated to be of order $4/N \approx 1.5 \times 10^{-5}$; and the rms statistical error to be $(NM)^{-1/2} \approx 1.7 \times 10^{-4}$.

Figure 5 is a log–log plot of the time-stepping error $|T_Q|$ against the time step Δt at the time $t = \frac{1}{4}$. For the frequency $\langle \omega \rangle$, the time-stepping error, T_ω, is essentially negligible. Even with the largest possible time step (i.e., $\Delta t = \frac{1}{4}$) the error is just 2.5×10^{-4}, and it is evident that T_ω varies as Δt^2.

Of the other statistics shown (k, $\langle u_1^2 \rangle$, $\langle u_1 u_2 \rangle$, and $\tilde{k}/k$), the time-stepping error in $\langle u_1^2 \rangle$ is the largest. This is less than 10^{-2}

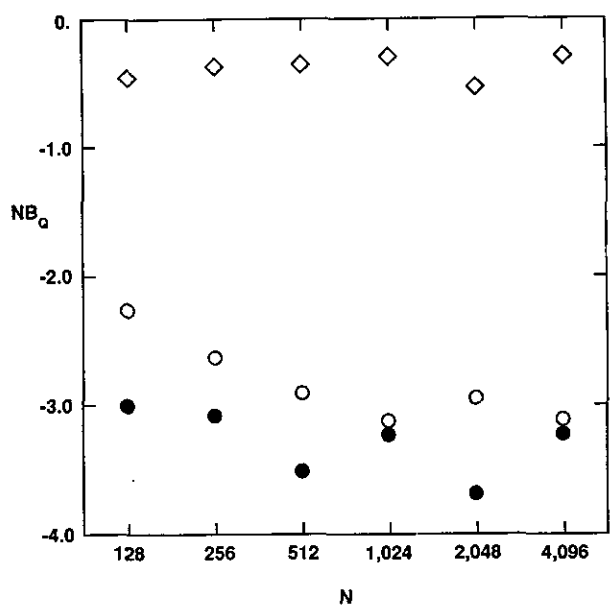

FIG. 4. Bias times N vs N: ○, k; ◇, $\langle u_1 u_2 \rangle$; ●, $\tilde{k}/k$ (homogeneous shear, $t = 1$, $\Delta t = \frac{1}{16}$).

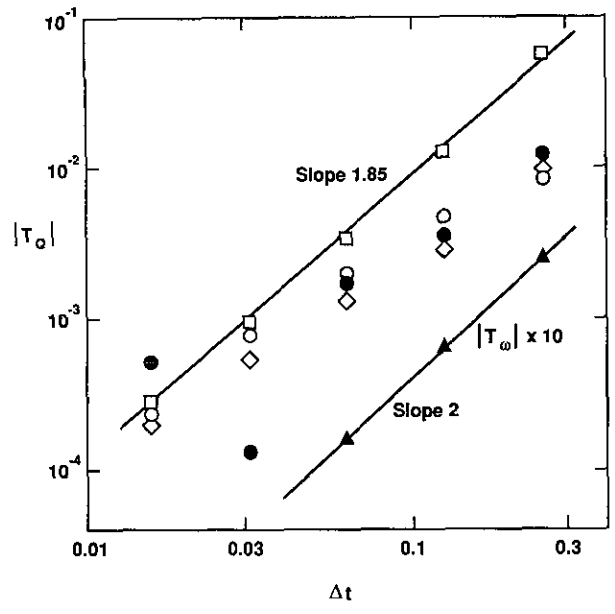

FIG. 5. Time-stepping error vs time step for homogeneous shear at $t = \frac{1}{4}$: ○, k; □, $\langle u_1^2 \rangle$; ◇, $\langle u_1 u_2 \rangle$; △, $\langle \omega \rangle (10 \times |T_\omega|)$; ●, $\tilde{k}/k$. Upper line has slope 1.85; lower line has slope 2.

and 10^{-3} for $\Delta t \leq \frac{1}{10}$ and $\Delta t \leq \frac{1}{32}$, respectively. It appears that $T_{u_1}^2$ varies approximately as $\Delta t^{1.85}$. On the other hand, the smaller errors, T_k and $T_{u_1 u_2}$, appear to vary as $\Delta t^{1.25}$.

For the statistics not shown (K and $\mu_{1/2}$) the time-stepping errors are smaller than the confidence interval in the results: for all $\Delta t \leq \frac{1}{4}$, with 95% confidence, $|T_K|$ is less than 3×10^{-3} and $|T_{\mu 1/2}|$ is less than 2×10^{-4}.

Figure 6 shows the same time-stepping errors at $t = 1$. Again $|T_\omega|$ is very small and varies as Δt^2. Of the other statistics, $\langle u_1 u_2 \rangle$ now has the dominant time-stepping error, which varies as $\Delta t^{1.75}$. Time steps of $\frac{1}{8}$ and $\frac{1}{32}$ suffice to reduce the time-stepping errors below 10^{-2} and 10^{-3}, respectively. As may be expected, taking a single step of size $\Delta t = 1$ produces large time-stepping errors; but nevertheless the method is stable. For $\Delta t = \frac{1}{2}$ and $\Delta t = \frac{1}{4}$ the errors are less than 0.05 and 0.025, respectively.

In summary, the results show that the numerical method is stable for very large time steps and that the time-stepping errors tend to zero as Δt tends to zero. This—together with the previously established results that NB_Q and S_Q remain finite as N tends to infinity—demonstrates the convergence of the method as a whole. Over the range of time steps investigated, the dominant time-stepping error increases as Δt^p, $p \geq 1\frac{3}{4}$. One percent accuracy (i.e., $|T_Q| \leq 0.01$) is achieved with $\Delta t \langle \omega(0) \rangle \leq \frac{1}{10}$.

6.5. *Bimodal Initial Condition*

The second test case, reported in this subsection, is designed to examine those aspects of the numerical method that are not seriously tested in sheared Gaussian turbulence. In particular, in this second case, the turbulence is distinctly non-Gaussian, and (with probability $\frac{1}{2}$) the important but singular initial condition $\omega(0) = 0$ is used.

In the absence of mean velocity gradients (i.e., $\Gamma_{ij} = 0$), the turbulence evolves from bimodal turbulent/non-turbulent initial conditions. The initial joint pdf can be written

$$f(\mathbf{v}, \theta; 0) = \tfrac{1}{2} f_t(\mathbf{v}, \theta; 0) + \tfrac{1}{2} f_n(\mathbf{v}, \theta; 0), \tag{121}$$

where f_t and f_n are the conditional joint pdf's of the turbulent and non-turbulent fluid, respectively. The non-turbulent fluid has the deterministic initial conditions: $u_1(0) = -1$; $u_2(0) = u_3(0) = \omega(0) = 0$. The turbulent fluid has the conditional means $\langle u_1(0) \rangle_t = \langle \omega(0) \rangle_t = 1$, $\langle u_2(0) \rangle_t = \langle u_3(0) \rangle_t = 0$; and $\mathbf{u}(0)$ and $\ln \omega(0)$ are joint-normally distributed with the identity covariance matrix. Thus the initial joint pdf is

$$f(\mathbf{v}, \theta; 0) = \frac{1}{2} \delta(v_1 + 1)\, \delta(v_2)\, \delta(v_3)\, \delta(\theta) + \frac{1}{8\pi^2 \theta} \exp\left\{ -\frac{1}{2} [(v_1 - 1)^2 + v_2^2 + v_3^2] - \frac{1}{2} \ln \theta - \frac{1}{4} \right\}. \tag{122}$$

The initial values of the monitored statistics are given in

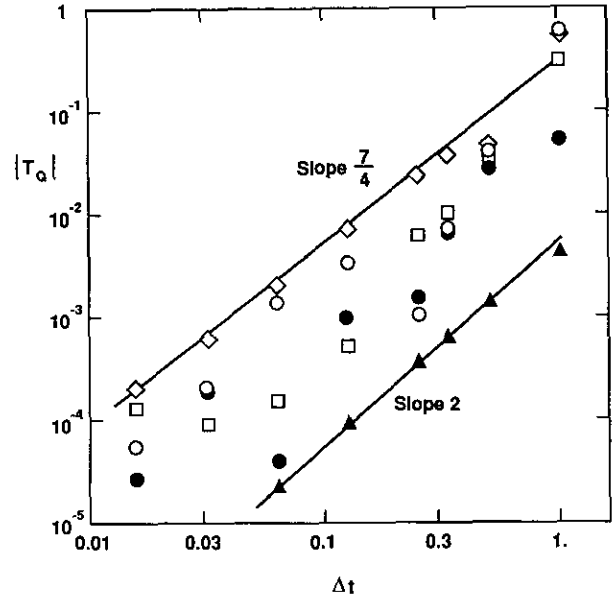

FIG. 6. Time-stepping error vs time step for homogeneous shear at $t = 1$; ○, k; □, $\langle u_1^2 \rangle$; ◇, $\langle u_1 u_2 \rangle$; △, $\langle \omega \rangle$. Upper line has slope $1\frac{3}{4}$; lower line has slope 2.

TABLE II

Statistics for the Bimodal Test Case

$\langle Q \rangle$	$\langle Q(0) \rangle$	$\langle Q(1) \rangle^a$	$S_Q{}^b$	$NB_Q{}^b$
k	$1\frac{1}{4}$	0.6037 ± 0.00016	0.29	−4.2
$\langle u_1^2 \rangle$	$1\frac{1}{2}$	0.4097 ± 0.00012	0.23	−2.6
$\langle u_2^2 \rangle$	$\frac{1}{2}$	0.3989 ± 0.00010	0.21	−3.0
K	$2\frac{4}{9}$	4.251 ± 0.0054	10.	−16.
$\langle \omega \rangle$	$\frac{1}{2}$	0.34958 ± 4 × 10^{-6}	0.008	−0.006
$\mu_{1/2}$	$\frac{1}{\sqrt{2}}e^{-1/8}$	0.7676 ± 0.0001	0.27	0.4
$\tilde{k}/k$	$1\frac{3}{5}$	1.6336 ± 0.0015	2.7	−12.

[a] Estimate of $\langle Q(1) \rangle$ obtained using Richardson extrapolation from results with $\Delta t = \frac{1}{64}$ (32 trials) and $\Delta t = \frac{1}{128}$ (64 trials), and $N = 2^{18}$. Statistical error estimates correspond to 95% confidence interval.

[b] Results obtained at $t = 1$ with $\Delta t = \frac{1}{16}$, $N = 128$–4096.

Table II. (For this case $\langle u_2^2 \rangle$ is monitored in place of $\langle u_1 u_2 \rangle$ which is identically zero.)

The evolution of the controlled and uncontrolled moments is shown on Figs. 7 and 8, respectively. Initially $\langle u_1^2 \rangle$ is three times $\langle u_2^2 \rangle$ because of the difference in the conditional mean velocities ($\langle u_1 \rangle_t = 1$, $\langle u_1 \rangle_n = -1$). The difference subsequently decreases quite rapidly as the turbulence tends towards isotropy. The non-Gaussian aspects of the turbulence are clear from Fig. 8. The kurtosis K is initially below the Gaussian value of 3, but soon increases to exceed 4 before decreasing towards 3. The ratio $\tilde{k}/k$ increases to a maximum of 1.8 before beginning to decrease to its asymptotic value of 1. Similarly $\mu_{1/2}$ gradually rises towards its asymptotic value of $e^{-\sigma^2/8} \approx 0.882$. At the end

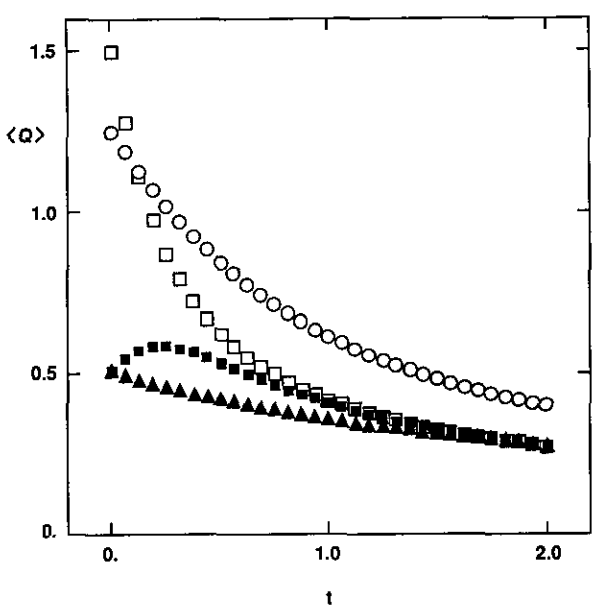

FIG. 7. Temporal evolution of controlled statistics for the bimodal test case: ○, k; □, $\langle u_1^2 \rangle$; □, $\langle u_2^2 \rangle$; △, $\langle \omega \rangle$ ($\Delta t = \frac{1}{16}$, $n = 2^{18}$).

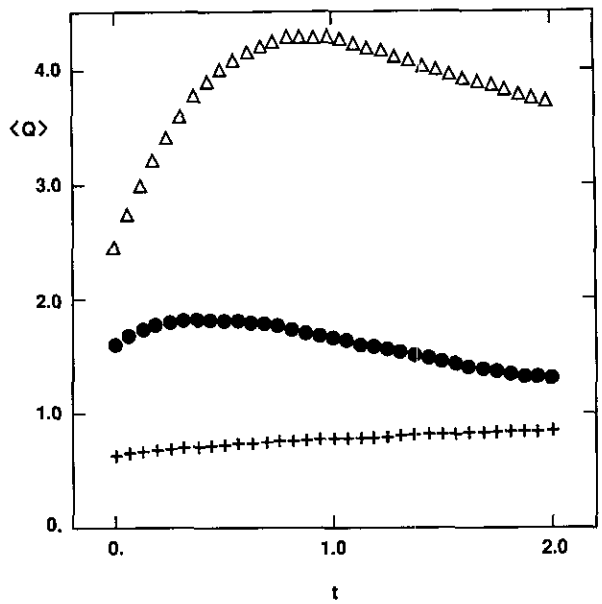

FIG. 8. Temporal evolution of uncontrolled statistics for the bimodal test case: △, $K = \langle u_1^4 \rangle / \langle u_1^2 \rangle^2$; +, $\mu_{1/2} = \langle (\omega / \langle \omega \rangle)^{1/2} \rangle$; ●, $\tilde{k}/k$ ($\Delta t = \frac{1}{16}$, $N = 2^{18}$).

of the observation period ($t = 2$) these statistics are still significantly different from their asymptotic values.

The numerical method is tested by examining statistics at $t = 1$. This time was selected because it allows a substantial evolution to take place, and yet the turbulence is still far from Gaussian.

As before, it is found that the standard errors S_Q vary slightly with Δt, but are essentially independent of N (at least for $N \geq 256$). Their values at $t = 1$ are given in Table II. For the Reynolds stresses, $S_Q/\langle Q \rangle$ is comparable to the values of the Gaussian case, i.e., about a half. But for K and $\tilde{k}/k$, the standard error is more than double.

The behavior of the bias is also similar to the previous case. Asymptotically B_Q varies linearly with N^{-1}, with the values of NB_Q given in Table II. For the Reynolds stresses and $\langle \omega \rangle$ the values are similar to the previous case, but those of K and $\tilde{k}/k$ are appreciably larger.

Although there is no reason to doubt it, for this case the question of convergence as Δt tends to zero cannot be addressed, because an exact solution is not available. However, by assuming that the method does indeed converge, we are able to study the dependence of the time-stepping errors T_Q on Δt. The converged ($\Delta t = 0$) solution is estimated using Richardson extrapolation based on results obtained with $\Delta t = \frac{1}{64}$ and $\Delta t = \frac{1}{128}$ and $N = 2^{18}$. Then, for $\Delta t > 0$, the time-stepping error T_Q is estimated as the departure from this extrapolated value.

Figure 9 is a log–log plot of time-stepping errors against Δt. As before, even with a single time step ($\Delta t = 1$) the time-stepping error in $\langle \omega \rangle (T_{\langle \omega \rangle})$ is remarkably small—less than 2×10^{-3}. And $T_{\langle \omega \rangle}$ is found to vary approximately as $\Delta t^{2.3}$.

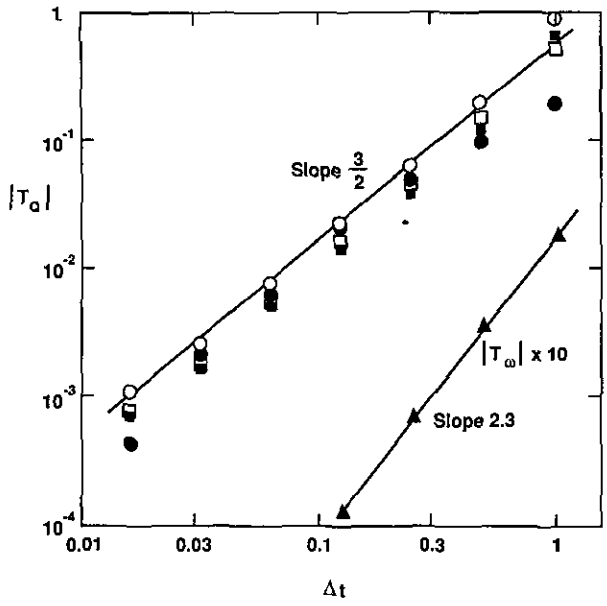

FIG. 9. Time-stepping error vs time step for the bimodal test at $t = 1$: ○, k; □, $\langle u_1^2 \rangle$; □, $\langle u_2^2 \rangle$; △, $\langle \omega \rangle (10 \times |T_\omega|)$; ●, $\tilde{k}/k$. Upper line has slope $1\frac{1}{2}$; lower line has slope 2.3.

Of the other statistics shown, the error in k is largest, although the others are similar in behavior and magnitude. For $\Delta t = \frac{1}{4}$, $\frac{1}{8}$, and $\frac{1}{16}$, the errors are 0.06, 0.025, and 0.008, respectively. Even for $\Delta t = 1$ (i.e., a single time step) the method is stable. The time-stepping error in these statistics appears to vary as $\Delta t^{3/2}$.

For $\Delta t \leq \frac{1}{8}$, the time-stepping errors in K and $\mu_{1/2}$ are zero, to within the confidence interval of the test.

6.6. *Computational Considerations*

For the zero-dimensional flows considered here, the computer requirements are extremely modest. For example, on a Silicon Graphics (SGI 4D 240 GTX) workstation, just 8 CPU seconds are required for a run with 1024 particles and 32 time steps. (Taking 3 Mflops as a nominal speed for the workstation, this implies about 700 floating-point operations per particle per time step.) From this figure, the requirements for multi-dimensional calculations can be roughly estimated by assuming that the time required is linearly proportional to the number of particle-steps taken. For example, for a 2D calculation with 100 particles in each of 1000 cells and 500 time steps, the estimated time required on the same workstation is about $3\frac{1}{2}$ h.

While one run with 1024 particles requires just 8 s of CPU time, to determine the time-stepping error to the required confidence level vastly more time is required. For example, the leftmost points on Fig. 6 were obtained by averaging over $M = 128$ independent trials, each with $2^{18} \sim 2.6 \times 10^5$ particles. These computations were performed on a 32-node Intel iPSC/860. The parallel implementation of the method—either partitioning the trials, or partitioning the particles—proved to be straightforward, with essentially 100% parallel efficiency [39].

7. DISCUSSION AND CONCLUSIONS

A numerical method has been developed to integrate the set of stochastic differential equations that form the basis of a pdf turbulence model. These equations present several challenges: they are stochastic; they contain two (sometimes disparate) time scales $\langle \omega \rangle^{-1}$ and $\langle \omega^* \rangle^{-1}$; there is a singular behavior for the initial condition $\omega^* = 0$; and the coefficients in the sde's contain statistical noise.

A simple two-stage predictor–corrector time-stepping strategy is adopted. The central idea behind the integration scheme is to transform and decompose the equations so that the stochastic components appear as strictly linear sde's. Then analytic solutions to these equations (with frozen coefficients) are used, thus ensuring stability and low time-stepping errors.

The numerical method has been implemented and comprehensively tested for two test cases. The results clearly demonstrate the stability of the method for large time steps, and its convergence as Δt tends to zero and N tends to infinity.

Three types of numerical error are identified: statistical error, S_Q; bias, B_Q; and time-stepping error, T_Q. The first two errors depend primarily upon N and scale as $S_Q \sim N^{-1/2}$ and $B_Q \sim N^{-1}$. Consequently, for sufficiently large N (typically $N > 200$ for the present tests) the statistical error dominates.

For the velocity equations, a variance-reduction technique has been developed, which is extremely effective at reducing the statistical error. For a given error tolerance, it reduces the CPU time required by more than a factor of 8. In the two test cases, with $N = 100$ the rms statistical error in the turbulent kinetic energy k is 7% and 3%, respectively. With $N = 1000$ it is 2% and less than 1%.

The second test case (with bimodal initial conditions) provides the more severe test of the time-stepping errors. With non-dimensional time steps of $\langle \omega \rangle \Delta t = \frac{1}{16}$ and $\frac{1}{32}$, the time-stepping errors in k are 2.5% and 0.8%, respectively. The dominant time-stepping errors appear to vary as $\Delta t^{3/2}$, whereas the same predictor–corrector scheme applied to ordinary differential equations would yield $T_Q \sim \Delta t^2$ (i.e., second-order accuracy). While second-order accurate methods for sde's are available (e.g., [28–30]), the present approach was adopted because of its stability properties. As observed in Section 3, the frequency ω^* of some particle can be expected to be 40 times the mean $\langle \omega \rangle$; and the characteristic time scale in the sde for $\mathbf{u}^*$ is $(\frac{3}{4} C_0 \omega^*)^{-1}$. Thus the apparently small time step $\langle \omega \rangle \Delta t = \frac{1}{16}$ may, in fact, be quite large for some particles, e.g.,

$$\frac{3}{4} C_0 \omega^* \Delta t = 2 \frac{5}{8} \left(\frac{\omega^*}{\langle \omega \rangle} \right) \langle \omega \rangle \Delta t \approx 6. \tag{123}$$

In convergence, stability, accuracy, and efficiency the numer-

ical method developed here is quite satisfactory. It provides the basic integration scheme for multi-dimensional particle methods to solve the velocity-frequency joint pdf equation for inhomogeneous turbulent flows.

APPENDIX A: ANALYTIC SOLUTION FOR SHEARED GAUSSIAN HOMOGENEOUS TURBULENCE

For the case considered (see Section 6.1), it can be deduced from Eq. (14) or (26) that $\langle\omega\rangle$ evolves by

$$\frac{d\langle\omega\rangle}{dt} = -\langle\omega\rangle^2 S_\omega, \tag{124}$$

where (from Eqs. (16), (107)) S_ω is constant:

$$S_\omega = -\tfrac{1}{2}\Gamma_0^2 C_{\omega 1} + C_{\omega 2}. \tag{125}$$

From the initial condition $\langle\omega(0)\rangle = 1$, the solution is

$$\langle\omega(t)\rangle = (1 + tS_\omega)^{-1}. \tag{126}$$

The Reynolds-stress equations are solved in the normalized time variable

$$\tau(t) \equiv \int_0^t \langle\omega(t')\rangle\, dt'. \tag{127}$$

From Eq. (125) we obtain

$$\tau(t) = S_\omega^{-1} \ln(1 + tS_\omega). \tag{128}$$

The evolution equation for the Reynolds stresses $\langle u_i u_j\rangle$ (obtained from Eq. (21) or (26)) is

$$\frac{d}{dt}\langle u_i u_j\rangle + \langle u_i u_l\rangle\Gamma_{jl} + \langle u_j u_l\rangle\Gamma_{il} = -\beta\langle\omega\rangle\left(\langle u_i u_j\rangle - \frac{2}{3}k\,\delta_{ij}\right) - \frac{2}{3}\langle\varepsilon\rangle\,\delta_{ij}, \tag{129}$$

where

$$\beta \equiv 1 + \tfrac{3}{2}C_0. \tag{130}$$

Substituting for Γ_{ij} (Eq. (107)) and transforming to the normalized time τ (Eq. (127)), we obtain the following linear set of equations:

$$\frac{d}{d\tau}\begin{bmatrix} k \\ \langle u_1 u_2\rangle \\ \langle u_2^2\rangle \end{bmatrix} = \begin{bmatrix} -1 & -\Gamma_0 & 0 \\ 0 & -\beta & -\Gamma_0 \\ C_0 & 0 & -\beta \end{bmatrix}\begin{bmatrix} k \\ \langle u_1 u_2\rangle \\ \langle u_2^2\rangle \end{bmatrix}. \tag{131}$$

This completely determines all the Reynolds stresses, since $\langle u_1 u_3\rangle$ and $\langle u_2 u_3\rangle$ are zero, $\langle u_3^2\rangle$ equals $\langle u_2^2\rangle$ and, hence, $\langle u_1^2\rangle = 2(k - \langle u_2^2\rangle)$.

The value of Γ_0 (Eq. (108)) is chosen so that one eigenvalue of the matrix in Eq. (131) is zero. It is then straightforward to solve the linear system to obtain the general solution

$$\begin{aligned}\begin{bmatrix} k \\ \Gamma_0\langle u_1 u_2\rangle \\ \Gamma_0^2\langle u_2^2\rangle \end{bmatrix} &= A_1\begin{bmatrix} 1 \\ -1 \\ \beta \end{bmatrix} \\ &+ e^{-(\beta+1/2)\tau}(A_2\cos(\alpha\tau) \\ &+ A_3\sin(\alpha\tau))\begin{bmatrix} 1 \\ \beta - \frac{1}{2} \\ -\frac{1}{2}\beta \end{bmatrix} \\ &+ e^{-(\beta+1/2)\tau}(A_2\sin(\alpha\tau) - A_3\cos(\alpha\tau))\begin{bmatrix} 0 \\ \alpha \\ \alpha\beta \end{bmatrix},\end{aligned} \tag{132}$$

where

$$\alpha = \sqrt{\beta - 1/4}. \tag{133}$$

The constants, determined by the initial conditions, are

$$A_1 = (\tfrac{3}{2} + \Gamma_0^2/\beta^2)/(1 + 2/\beta), \tag{134}$$

$$A_2 = \tfrac{3}{2} - A_1 \tag{135}$$

and

$$A_3 = (\tfrac{3}{2}A_1 - \tfrac{3}{4} - \Gamma_0^2/\beta)/\alpha. \tag{136}$$

ACKNOWLEDGMENTS

This work is supported in part by Contract "Combustion Design Model Evaluation" (F33615-87-C-2821) from the U.S. Air Force, Wright Aeronautical Laboratories, to Allison Engine Company, and, in part, by Grant CTS-9113236 from the National Science Foundation. Computations were performed using the resources of the Cornell Theory Center, which receives major funding from the National Science Foundation and IBM Corporation, with additional support from New York State Science and Technology Foundation and members of the Corporate Research Institute.

REFERENCES

1. J. L. Lumley, *Whither Turbulence? Turbulence at the Crossroads* (Springer-Verlag, Berlin, 1990).
2. D. C. Wilcox, *Turbulence Modeling for CFD* (DCW Industries, LaCañada, CA, 1993).
3. W. P. Jones and B. E. Launder, *Int. J. Heat Mass Transfer* **15**, 301 (1972).

4. B. E. Launder and D. B. Spalding, *Mathematical Models of Turbulence* (Academic Press, New York, 1972).
5. S. J. Kline, B. J. Cantwell, and G. M. Lilley, *AFOSR-HTTM-Stanford Conference on Turbulent Flows*, Stanford University, 1981.
6. B. E. Launder, *Appl. Sci. Res.* **48,** 247 (1991).
7. E. E. O'Brien, *Turbulent Reactive Flows* (Springer-Verlag, Berlin, 1980).
8. S. B. Pope, *Prog. Energy Combust. Sci.* **11,** 119 (1985).
9. S. B. Pope, *23rd International Symposium on Combustion* (The Combustion Institute, Pittsburgh, 1990), p. 591.
10. C. Dopazo, technical report, University of Zaragoza, 1991.
11. S. B. Pope, *Annu. Rev. Fluid Mech.* **26,** 23 (1994).
12. S. B. Pope and Y. L. Chen, *Phys. Fluids A* **2,** 1437 (1990).
13. S. B. Pope. *Phys. Fluids A* **3,** 1947 (1991).
14. W. P. Jones and J. H. Whitelaw, *20th International Symposium on Combustion* (The Combustion Institute, Pittsburgh, 1985), p. 223.
15. S. M. Correa and W. Shyy, *Prog. Energy Combust. Sci.* **13,** 249 (1987).
16. C. H. Priddin and J. Coupland, *Combust. Sci. Technol.* **58,** 119 (1988).
17. S. B. Pope, *Combust. Sci. Technol.* **25,** 159 (1981).
18. T. V. Nguyen and S. B. Pope, *Combust. Sci. Technol.* **42,** 13 (1984).
19. D. C. Haworth and S. B. Pope, *J. Comput. Phys.* **72,** 311 (1987).
20. J.-Y. Chen, R. W. Dibble, and R. W. Bilger, *23rd International Symposium on Combustion* (The Combustion Institute, Philadelphia, 1990), p. 775.
21. M. S. Anand, S. B. Pope, and H. C. Mongia, *Turbulent Reactive Flows*, Vol. 40 (Springer-Verlag, Berlin, 1989), p. 672.
22. D. C. Haworth and S. H. El Tahry, *AIAA J.* **29,** 208 (1991).
23. D. Roekaerts, *Appl. Sci. Res.* **48,** 271 (1991).
24. S. M. Correa and S. B. Pope, *24th International Symposium on Combustion* (The Combustion Institute, Philadelphia, 1992), p. 279.
25. A. T. Norris and S. B. Pope, *25th International Symposium on Combustion* (The Combustion Institute, Pittsburgh, 1995), in press.
26. G. N. Mil'shtein, *Theory Probab. Its Appl.* **30,** 750 (1985).
27. H. S. Greenside and E. Helfand, *Bell Syst. Tech. J.* **60,** 1927 (1981).
28. D. Talay, *Stochastics* **9,** 275 (1983).
29. D. C. Haworth and S. B. Pope, *Stochastic Anal. Appl.* **4,** 151 (1986).
30. P. E. Kloeden and E. Platen, *Numerical Solution of Stochastic Differential Equation* (Springer-Verlag, Berlin, 1992).
31. C. W. Gardiner, *Handbook of Stochastic Methods* (Springer-Verlag, Berlin, 1985).
32. D. C. Haworth and S. B. Pope, *Phys. Fluids* **29,** 387 (1986).
33. D. C. Haworth and S. B. Pope, *Phys. Fluids* **30,** 1026 (1987).
34. S. B. Pope, *Phys. Fluids* **6,** 973 (1994).
35. S. Karlin and H. M. Taylor, *A Second Course in Stochastic Processes* (Academic Press, New York, 1981).
36. D. C. Handscomb and J. M. Hammersley, *Monte Carlo Methods* (Methuen, New York, 1965).
37. M. H. Kalos and P. A. Whitlock, *Monte Carlo Methods* (Wiley, New York, 1986).
38. L. Arnold, *Stochastic Differential Equations: Theory and Applications* (Wiley, New York, 1974).
39. S. B. Pope, in *Turbulence and Molecular Processes in Combustion*, edited by T. Takeno (Elsevier, Amsterdam, 1993).